Redox Biology 69 (2024) 102986

Contents lists available at ScienceDirect

Redox Biology

journal homepage: www.elsevier.com/locate/redox

Estrogen genotoxicity causes preferential development of Fuchs endothelial corneal dystrophy in females

Varun Kumar [a,2,1], Neha Deshpande [a,1], Mohit Parekh [a], Raymond Wong [a], Shazia Ashraf [a], Muhammad Zahid [b], Hanna Hui [a], Annie Miall [a], Sylvie Kimpton [a], Marianne O. Price [c], Francis W. Price Jr. [c], Frank J. Gonzalez [d], Eleanor Rogan [b], Ula V. Jurkunas [a,*]

[a] Schepens Eye Research Institute of Massachusetts Eye and Ear, Department of Ophthalmology, Harvard Medical School, Boston, MA, 02115, USA
[b] Department of Environmental, Agricultural and Occupational Health, College of Public Health, University of Nebraska Medical Center, Omaha, NE, 68198-4388, USA
[c] Price Vision Group and Cornea Research Foundation of America, Indianapolis, IN, USA
[d] Center for Cancer Research, National Cancer Institute, Bethesda, MD, USA

ARTICLE INFO

Keywords:
Fuchs endothelial corneal dystrophy
Estrogen metabolism
TMS
CYP1B1
NQO1
Mitochondrial DNA damage
Berberine
Estrogen-DNA adducts
Catechol estrogen
Oxidized estrogen
Ultraviolet-A

ABSTRACT

Fuchs endothelial corneal dystrophy (FECD) is a genetically complex, age-related, female-predominant disorder characterized by loss of post-mitotic corneal endothelial cells (CEnCs). Ultraviolet-A (UVA) light has been shown to recapitulate the morphological and molecular changes seen in FECD to a greater extent in females than males, by triggering CYP1B1 upregulation in females. Herein, we investigated the mechanism of greater CEnC susceptibility to UVA in females by studying estrogen metabolism in response to UVA in the cornea. Loss of NAD(P)H quinone oxidoreductase 1 (NQO1) resulted in increased production of estrogen metabolites and mitochondrial-DNA adducts, with a higher CEnC loss in *Nqo1*$^{-/-}$ female compared to wild-type male and female mice. The CYP1B1 inhibitors, *trans*-2,3′,4,5′-tetramethoxystilbene (TMS) and berberine, rescued CEnC loss. Injection of wild-type male mice with estrogen (E2; 17β-estradiol) increased CEnC loss, followed by increased production of estrogen metabolites and mitochondrial DNA (mtDNA) damage, not seen in E2-treated *Cyp1b1*$^{-/-}$male mice. This study demonstrates that the endo-degenerative phenotype is driven by estrogen metabolite-dependent CEnC loss that is exacerbated in the absence of NQO1; thus, explaining the mechanism accounting for the higher incidence of FECD in females. The mitigation of estrogen-adduct production by CYP1B1 inhibitors could serve as a novel therapeutic strategy for FECD.

1. Introduction

Corneal endothelium (CE) is a monolayer of hexagonal cells lining the posterior surface of the cornea that maintains corneal transparency by constant pumping of ions and providing a barrier between the corneal stroma and the aqueous humor. Corneal endothelial cells (CEnCs) are arrested in a postmitotic state and have a limited proliferative capacity *in vivo* [1,2]. Fuchs endothelial corneal dystrophy (FECD) is an age-related, genetically heterogeneous, oxidative stress disorder resulting in progressive loss of CEnCs and ensuing corneal edema [3,4]. Progressive loss of CEnCs, mainly via apoptosis [5], is accompanied by changes in the cellular junctional complexes [5–7] and deposition of extracellular matrix excrescences in the Descemet's membrane (DM), known as guttae [8], which are notably the main characteristic of FECD (Fig. 1a). FECD affects approximately 4 % of the U.S. population over 40 years of age, with a significantly higher incidence (3- to 4-fold) in women compared to males, suggesting a possible hormonal role in the sex-driven differences of the disease pathogenesis [9–11]. FECD is most commonly associated with expansion of the intronic trinucleotide CTG repeats (>40) in the TCF4 gene [12], accounting for about 70 % of all FECD cases in the European and U.S. populations. Despite progress in studies on the genetic underpinnings of FECD, corneal transplantation is the only treatment for FECD, and it is the major cause of allogeneic corneal transplants performed in the U.S. and worldwide [13]. The lack of pharmacological treatments for FECD presents an unmet need for studies that explore the molecular mechanisms involved in the CEnC

* Corresponding author.
E-mail address: ula_jurkunas@meei.harvard.edu (U.V. Jurkunas).
[1] These authors have equally contributed.
[2] Present address: Icahn School of Medicine at Mount Sinai, New York City, NY, 10029, USA.

https://doi.org/10.1016/j.redox.2023.102986
Received 15 November 2023; Received in revised form 1 December 2023; Accepted 3 December 2023
Available online 6 December 2023

loss, including the contribution of female sex in its pathogenesis.

In multiple studies, female sex, in addition to age, has been reported to be the most significant risk factor for FECD development [11,14,15]. Notably, development of guttae, which lead to CEnC loss, is significantly higher in females compared to males across various racial populations. For example, the Reykjavik study detected guttae prevalence of 11 % in females and 7 % in males in the Icelandic population [11], while other studies showed a guttae prevalence of 5.8 % in females and 2.4 % in males in Japanese population and 8.5 % in females and 4.4 % in males in Chinese Singaporeans [9–11,15]. A retrospective analysis of 546 corneal transplants performed for FECD found that women represent 77 % of patients [16,17]. Additionally, smoking and diabetes, the major risk factors for FECD, show an increased effect on severity and advanced FECD stage in a female compared to male cohort [14]. Even though females are more affected than males by FECD, the regulators of sex-driven differences in the disease pathogenesis are unknown.

Various studies have implicated the role of oxidative stress in FECD pathogenesis [4,18–21]. Post-mitotically arrested CEnCs engage in high metabolic activity due to their ionic pump function, facilitated by a high density of mitochondria, which increases the susceptibility to oxidative stress and related molecular changes. Previously, we and others have demonstrated that acquired oxidative DNA damage and a pro-oxidant environment contribute significantly to the development of FECD [22–24]. There is reduced expression of nuclear factor erythroid 2-related factor-2 (NRF2), a critical redox-sensitive transcription factor, and its downstream antioxidant defense enzyme NAD(P)H quinone

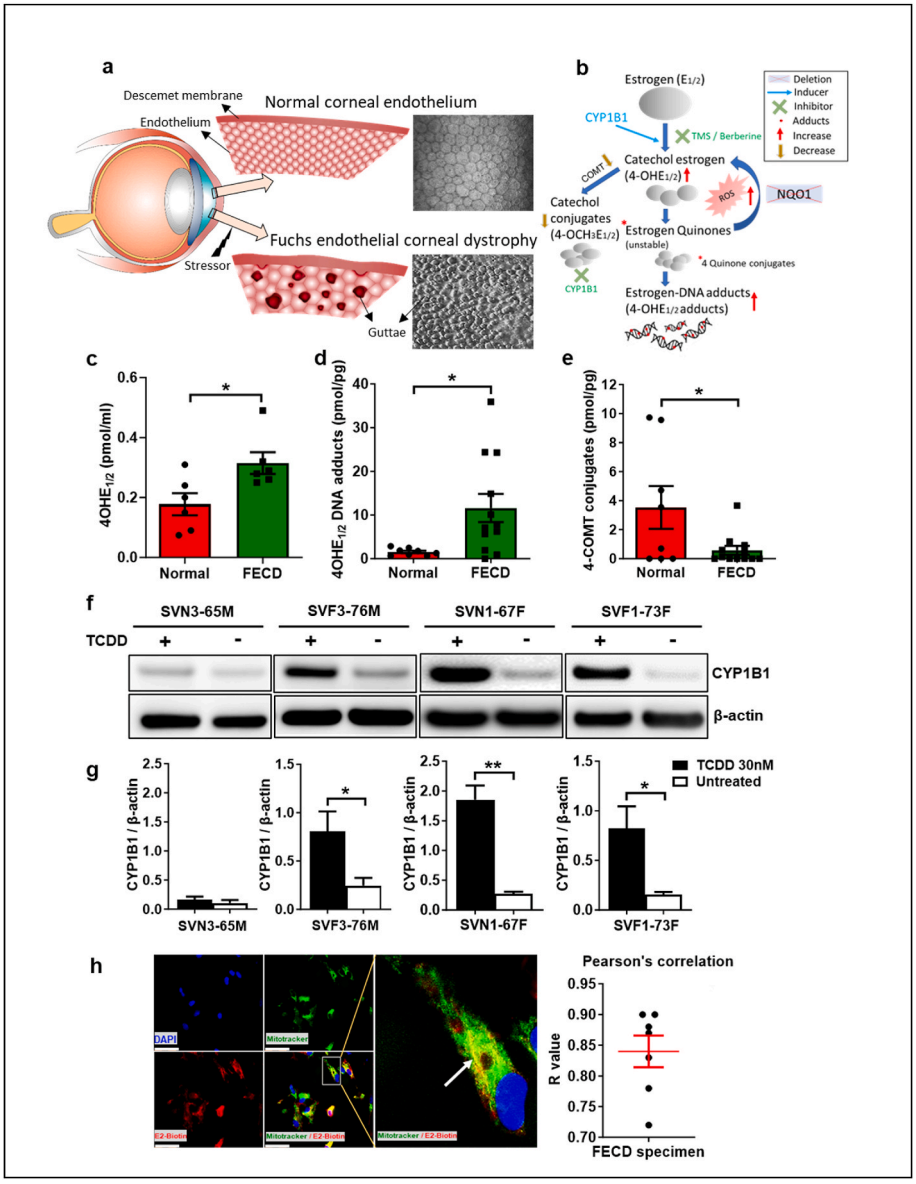

Fig. 1. CYP1B1-related metabolites and effect of estrogen treatment on mitochondria of human corneal endothelial cells and CYP1B1 protein expression in normal and FECD cell lines. (a) Illustration of the human eye showing normal compared to FECD corneal endothelium. (b) Effect of NQO1 deletion on CYP1B1 expression, and the role of CYP1B1 specific inhibitor, TMS and NRF2-ARE-NQO1 agonist, berberine in estrogen metabolism. UPLC/MS/MS analysis of CYP1B1-related metabolites showing upregulation of (c) harmful catechol estrogens ($4\text{-OHE}_{1/2}$) in aqueous humor (n = 6,*p < 0.05; normal and FECD), (d) increased estrogen DNA adducts ($4\text{-OHE}_{1/2}$-DNA), (e) downregulation of non-harmful $4\text{-OHE}_{1/2}$ catechol conjugates in *ex vivo* corneal endothelial tissue of FECD (pooled n = 12, *p < 0.05) compared to normal samples (non-pooled n = 8,*p < 0.05). (f) Expression of CYP1B1 protein in normal male (SVN3-65M), FECD male (SVF3-76M), normal female (SVN1-67F), and FECD female (SVF1-73F) cell lines in response to 2,3,7,8 -Tetrachlorodibenzo-p-dioxin (TCDD, 30 nM). (g) Bar graph showing significantly increased CYP1B1 expression in SVF3-76M, SVN1-67F and SVF1-73F post TCDD (n = 3,*p < 0.05,**p < 0.01). (h) FECD *ex vivo* tissue (n = 4) showing exogenous estrogen (E2-biotin, red) colocalized (yellow) to mitochondria (MitoTracker, green) represented by Pearson's correlation; stained for nucleus (DAPI, blue).

oxidoreductase 1 (NQO1), leading to a defective oxidant-antioxidant system and oxidative stress in FECD [4,18–21]. NRF2 activates NQO1 expression by binding to the antioxidant response element (ARE) sequence in the *NQO1* upstream promoter region [25,26]. NQO1 is a highly inducible cytoprotective flavoprotein that performs the catalytic reduction of quinones and nitroaromatic compounds, thereby limiting the formation of reactive oxygen species (ROS) and free radicals in the cellular environment [27]. Besides ROS, endogenous estrogen quinones (E_2-3,4-Q) are also substrates of NQO1, where it catalyzes the reduction of quinone back to catechol estrogen, 4-hydroxyestradiol (4-$OHE_{1/2}$) [28]. This diverts the quinones from binding to DNA and prevents the generation of harmful depurinating estrogen-DNA adducts. Furthermore, the neutralizing enzyme catechol-O-methyl transferase (COMT) converts catechol estrogen into nonreactive and non-toxic methoxy estrogen conjugates (4-$OCH_3E_{1/2}$) (Fig. 1b) [29].

Our group recently established a nongenetic FECD animal model based on the physiological outcome of FECD susceptibility to oxidative stress [7]. We have shown that exposure to ultraviolet-A (UVA) light, which is a physiological stressor of corneal endothelium, causes a greater FECD phenotype, i.e. loss of junctional contacts, extracellular matrix deposition, and CEnC loss, in female compared to male mice due to altered estrogen metabolism, recapitulating greater incidence of FECD in females [7]. The sex-dependent effect of UVA was associated with activation of CYP1B1 and induction of reactive estrogen metabolite production; however, a direct mechanistic link between defective antioxidant system, mainly NRF2-NQO1, and increased production of estrogen DNA adducts in causing a higher prevalence of FECD in females has not been investigated [7,30] (Fig. 1b). Many diseases such as lymphoma, breast and prostate cancers demonstrate an unbalanced metabolism of endogenous estrogens resulting in the accumulation of harmful depurinating DNA adducts [31]. Specifically, aberrant endogenous estrogen hormones increase breast cancer risk due to cytochrome P450 (CYP) 1B1 (CYP1B1)-mediated oxidation of estrogens to reactive quinones, which generate estrogen-DNA adducts leading to DNA damage [31,32]. CYP1B1 catalyzes the 4-hydroxylation of estrone (E_1) and estradiol (E_2) into catechol estrogens 4-$OHE_{1/2}$, favoring estrogen quinone [$E_1(E_2)$-3,4-Q] formation. CYP1B1 is expressed in adult tissues with high expression in estrogen-related tissues in females [33,34]. Also, CYP expression varies between males and females [34].

In this study, we investigated the involvement of CYP1B1 and NQO1 in driving sex-dependent differences in corneal endothelial (CE) susceptibility to UVA in FECD. First, we found marked increases of CYP1B1-related estrogen metabolites in human FECD aqueous humor and tissues containing endothelium Descemet's membrane (EDM). Second, irradiation of genetically modified mouse lines, namely, *Nqo1*$^{-/-}$ and *Cyp1b1*$^{-/-}$ mice, revealed that *Nqo1*$^{-/-}$ female mice carry greater susceptibility to CE cell loss than male mice, due to lack of neutralization of estrogen metabolites. Next, we developed the first ocular E2-treated male mouse model and determined that systemic administration of estrogen causes a significant estrogen metabolite production in the CEnCs and aqueous humor *in vivo*, creating a tool to study relative effects of estrogen in female predominance of FECD. Estrogen injection of male mice augmented their ocular response to UVA irradiation, that was mitigated in *Cyp1b1*$^{-/-}$ male mice. Similarly, we have employed pharmacological interventions to augment NQO1 (via berberine) and inhibit CYP1B1 (via TMS) levels *in vivo* by studying their therapeutic potential against FECD. Since mitochondrial DNA (mtDNA) damage was the main differentiating factor in the greater female susceptibility to UVA-induced cell loss [7], we further investigated the mitochondrial localization of estrogen and estrogen-mediated mtDNA damage in response to UVA-induced redox imbalance, compounded by loss of NQO1. This study provides mechanistic insight into the role of oxidative stress involving CYP1B1-mediated estrogen genotoxicity during oxidant-antioxidant imbalance seen in FECD.

2. Materials and methods

2.1. Human tissue

This study was conducted according to the Declaration of Helsinki and approved by the Massachusetts Eye and Ear Institutional Review Board. Written and informed consent was obtained from patients undergoing surgical treatment for FECD. Post-keratoplasty specimens were procured from surgeries performed at Price Vision Group (Indianapolis, IN) and Massachusetts Eye and Ear Hospital (Boston, MA). Normal donor corneas harvested and preserved in hypothermic storage media within 24 h of death were obtained from Eversight Eye Bank (Ann Arbor, MI) based on criteria reported in our previous studies [21,35]. See Table 1 for further details on human specimens used in this study. Human aqueous humor was collected during cataract or transplant surgeries from normal or FECD patients respectively. Briefly, a 1 mm paracentesis was made in the peripheral cornea and the tip of a 30-gauge cannula was inserted through the paracentesis tract into the mid-anterior chamber. Small volume of aqueous humor (50–100 μL) was slowly aspirated. Aspiration was stopped as soon as the anterior chamber began to shallow. The aqueous humor specimens were placed on dry ice and stored at −80°C.

2.2. Animals

Nqo1$^{-/-}$ (PMID: 9516435) and *Cyp1b1*$^{-/-}$ mice (PMID: 10051580) were described in earlier studies. Healthy, live breeders of *Nqo1*$^{-/-}$ and *Cyp1b1*$^{-/-}$ mice were generated at Charles River (Wilmington, MA) by embryo reconstitution and crossing with healthy wild-type-C57BL6/N female mice, respectively. Monogamous pairs consisting of one male and one female mouse were crossed as per a heterozygous X heterozygous breeding scheme and the litters were genotyped by PCR to identify knockouts. Mice were housed at Schepens Eye Research Institute, Boston, USA, in a controlled environment with constant temperature, 12-h light/dark cycle, and food and water available ad libitum. Mice were anesthetized with a combined dose of ketamine (100 mg/kg) and xylazine (20 mg/kg) administered intraperitoneally (IP). Female mice were irradiated at the proestrus stage [36]. Animal studies were in accordance with the ARVO Statement for the Use of Animals in Ophthalmic and Visual Research as well as the NIH Guide for the Care and Use of Animals and were performed at Schepens Eye Research Institute (SERI) with approval from SERI Institutional Animal Care and Use Committees IACUC.

2.3. UVA irradiation of mouse Cornea

The method and details of UVA irradiation were described in our earlier publication [7]. Briefly, a UVA LED light source (M365LP1; Thorlabs, USA) with an emission peak of 365 nm light, 8 nm bandwidth (FWHM), and irradiance of 398 mW/cm^2 was focused down to a 4 mm diameter illumination spot onto the mouse cornea. The time of UVA exposure was adjusted to deliver the appropriate fluence (20 min 57 s for 500 J/cm^2) as measured with a thermal power sensor head (S425C, Thorlabs, USA) and energy meter console (PM100D, Thorlabs). The

Table 1
Cornea donor information.

	Normal		FECD	
	Female	Male	Female	Male
Age, y[a]	64 ± 8	58 ± 10	67 ± 1	68 ± 6
Tissue donors	4	4	24[b]	24[b]
Aqueous humor donors	3	3	3	3
Preservation time, days	9.8	9.5	4.8	4

[a] Average age in years with standard deviation shown.
[b] Four tissue donors were pooled per sample.

right eye (OD) was irradiated, while the contralateral eye (OS) served as untreated control and was covered with retention drapes (SpaceDrapes, Inc., USA). Mouse eyes were enucleated in sterile PBS, and corneas were isolated, snap-frozen, and sent for estrogen metabolite analysis or Western blot following treatment with vehicle or drugs.

2.4. TMS, berberine, and estrogen treatment

For the specific inhibition of CYP1B1, 2,4,3′,5′-tetramethoxystilbene (TMS) (1.5 mg/kg) (#10038, Cayman Chemicals, USA) [37–39] or the vehicle, dimethyl sulfoxide (DMSO) (#D2650, Sigma Aldrich, USA), was administered (IP) three times a week for two weeks in both *Nqo1*$^{+/+}$ and *Nqo1*$^{-/-}$ mice. Berberine (activation of NRF2 and inhibition of CYP1B1) (10 mg/kg) (#14050, Sigma Aldrich, USA) or the vehicle, cyclodextrin (#332593, Sigma Aldrich, USA) was injected (IP) once a week for up to three weeks starting immediately after UVA. For determining the effect of estrogen in *Cyp1b1*$^{+/+}$ and *Cyp1b1*$^{-/-}$ male mice, cyclodextrin-encapsulated 17β-estradiol (E2) (0.4 mg/kg) (#E4389, Sigma Aldrich, USA) or cyclodextrin (vehicle) was injected (IP) three times a week for four weeks after UVA irradiation. A similar dose of estradiol was shown to regulate inflammatory changes caused by asthma in male mice [40] and neurodegenerative changes in male rats [41].

2.5. UVA irradiation of *NQO1*$^{+/+}$ and *NQO1*$^{-/-}$ cell lines in vitro

Two 19.5-inch tubes (XX-15L; Analytic Jena US LLC) emitting 365 nm light (irradiance: 14.77 mW/cm^2) were used to irradiate *NQO1*$^{+/+}$ and *NQO1*$^{-/-}$ cell lines in 6-well culture plates with estrogen-free Chen's media (modified Chen's). The fluence delivered was 5 J/cm^2 (5 min 33 s) or 10 J/cm^2 (11 min 06 s) at 10 cm from the light source. After irradiation, the cells were recovered in the same media for 24 h at 37 °C with 5 % CO_2 and harvested for mitochondrial isolation using a mitochondria isolation kit (#K256, Bio Vision, USA).

2.6. Western blot analysis

Whole cell extracts from mouse corneal cups or *NQO1*$^{+/+}$ and *NQO1*$^{-/-}$ cell lines were taken as described in earlier publications [7, 30]. Briefly, proteins were loaded onto 4–12 % Bis-Tris NuPAGE gels (#NP0336, Thermo Fisher Scientific, USA), run, and transferred to polyvinylidene difluoride membrane (PVDF), blocked with 5 % non-fat dry milk, probed with primary antibodies overnight, then exposed to 1-h secondary antibody next day and finally probed with Super Signal West Pico or Femto (#34577 or # 34096, Thermo Fisher Scientific, USA). Densitometry was performed using Image J software (NIH, USA). The primary antibodies used were NQO1 (1:1000, #ab2346, Abcam, USA), Cytochrome *c* (1: 1000, #11940, Cell Signaling, USA), VDAC (1: 1000, #4661, Cell Signaling, USA), Actin (1: 5000, #A1978, Sigma, USA), Tom20 (1: 1000, #sc-17764, Santa Cruz Biotechnology, USA), CYP1B1 (1:600, #18505-1-AP, Proteintech, USA), GAPDH (1:1000, #G9545, Sigma, USA), COMT (1:1000, #AB5873-I, Sigma, USA) and secondary antibodies were horseradish peroxidase-conjugated mouse anti-rabbit IgG (1:1000, #sc-2357), anti-mouse IgG (1:1000, #sc-516102), and mouse anti-goat (1:1000, sc-2354), from Santa Cruz Biotechnology Inc., USA.

2.7. Immunohistochemistry

For *in vitro* colocalization studies, *NQO1*$^{+/+}$ and *NQO1*$^{-/-}$ cells were cultured on a 4-well chamber slide that was pre-coated with fibronectin collagen (FNC) coating mix (#0407, AthenaES, USA) for 24 h in Chen's media at a plating density of 1X10^5/1.7 cm^2. The cells were refreshed with modified Chen's media containing 0.3 μM of biotin-labeled estrogen (E2-biotin) complex (#MBS537732, My BioSource, USA) followed by treatment with or without 5 J/cm^2 UVA and recovered after 6 h of incubation in the same media. The treated cells on the slides were fixed with 4 % paraformaldehyde (PFA) at room temperature (RT) for 15 min and permeabilized with 0.25 % Triton-X100 for 10 min at RT, followed by blocking with 10 % normal goat and donkey serum (1:1) for 1 h at RT. The cells were incubated with anti-biotin (#ab53494, Abcam, USA) and Tom-20 (#sc-136211, Santa Cruz, USA) antibodies diluted in 5 % bovine serum albumin (BSA) and left overnight at 4°C in the dark. The following day, secondary antibodies (1: 500, donkey anti-rabbit FITC, #ab150073, Abcam, USA and 1:500, goat anti-mouse 568, #ab175473, Abcam, USA) were added. The cells were washed at least three times with 1 % BSA after each primary and secondary incubation step. The cells were incubated for 1 h in secondary antibody at RT before mounting with DAPI (VectaShield, Vectorlabs, USA). Images were acquired using Leica SP8 confocal microscope (Leica microsystems), the cells were analyzed for Pearson's correlation, and the R-value was determined using Coloc 2 plugin in ImageJ software (NIH, USA). For *ex vivo* immunostaining and colocalization studies, cornea-scleral rims from healthy human cadaveric donors and FECD patients were obtained. Following a standard DMEK peeling with a scoring technique, EDM tissue from the cadaveric donor was obtained. EDM from both, the healthy (69 year-old female, 63 year-old male) and FECD (30 year-old female, 78 year-old female) tissues were treated with 0.3 μM exogenous estrogen labeled with biotin (E2-biotin) [42] in modified Chen's media and incubated for 6 h. We did not detect mitochondrial fragmentation with 0.3 μM of E2-biotin, suggesting a non-toxic dose range, as shown in other studies [42]. The tissues were washed and fixed with 4 % PFA overnight at 4 °C followed by the same staining process and concentrations described above. At the end of the staining, the tissues were flat mounted on microscope glass slides with endothelium facing upwards, imaged using Leica SP8 confocal microscope, and analyzed with coloc2 plugin in ImageJ, as described above. To detect the apurinic/abasic sites, *NQO1*$^{+/+}$ and *NQO1*$^{-/-}$ cells were cultured as above, treated with 5 J/cm^2 UVA in PBS, and recovered after 6 h of incubation in modified Chen's media. The immunohistochemistry protocol (as described above) was followed with minor modifications that included sequential blocking of the cells with 10 % goat serum, Avidin, and Biotin (1 h each) (#SP-2001, Avidin/Biotin blocking kit, Vector Laboratories) in a dry incubator (37 °C), incubation with primary antibody (#A10550, 0.1 mg/ml, aldehyde reactive probe; ARP, Invitrogen, USA) and Tom20 (1: 1000, #sc-17764, Santa Cruz, USA) overnight at 4 °C followed by secondary antibody (1: 200, #SA1001, Streptavidin conjugated FITC, Invitrogen, USA; 1: 500, #ab175471, goat anti-rabbit Alexa fluor 568, Abcam, USA). The images were acquired and analyzed following the same settings as described above.

2.8. In vivo imaging

Mice were anesthetized as described earlier, and the corneal images were taken using a slit lamp biomicroscope attached to a camera (Nikon D100, Tokyo, Japan). The epithelial cell integrity was assessed by observing punctate staining under cobalt blue light using fluorescein (1 μL in 2.5 % PBS; Sigma Aldrich, USA) applied topically onto the lateral conjunctival sac. Anterior segment images were taken using anterior segment optical coherence tomography (OCT) (Bioptigen Spectral Domain Ophthalmic Imaging System Envisu R2200) with a 12 mm telecentric lens to scan the cornea. Central corneal thickness was measured using the inbuilt software in the OCT. For imaging the CE, mice were wrapped with heat retention drapes on the platform that holds them securely and then imaged by laser scanning *in vivo* confocal microscopy using the Heidelberg Retina Tomograph III (HRT III) with Rostock Corneal Module (RCM) (Heidelberg Engineering). The laser confocal microscope acquires 2D images representing a coronal cornea section of 400 × 400 μm (160,000 μm^2) at selectable corneal depth. Acquired images comprise 384 X 384 pixels with a lateral resolution of 1 μm per pixel. Digital images were stored on a computer workstation at 3 frames per sec.

2.9. Corneal endothelial density

The corneal endothelial (CE) density was obtained at weeks 1, 2, and 4 post-UVA and analyzed by a semi-automated cell counter in the Heidelberg Eye Explorer, version 1.3.0 (Heidelberg Engineering GmbH) inbuilt in HRT3 software. The average cell density was calculated from 3 HRT images collected from each mouse in each group of 5–7 mice. For each image, an area with at least 50 cells was considered for counting. Two blinded observers performed the CE density.

2.10. DNA damage analysis

Genomic DNA was isolated from *NQO1*$^{+/+}$ and *NQO1*$^{-/-}$ cell line or estrogen-treated *Cyp1b1*$^{+/+}$ and *Cyp1b1*$^{-/-}$ mice 24 h post-UVA using Genomic tip-20/G (#10223, Qiagen). Long amplicon-quantitative polymerase chain reaction (LA-qPCR) analysis for mitochondria (mt) DNA and nuclear (n)DNA was performed as previously described [43].

2.11. ROS measurement assay

Extracellular H_2O_2 levels in the mouse aqueous humor (AH) were measured as described previously [7]. Mouse AH was collected from the anterior chamber using a capillary needle and H_2O_2 levels were assayed using Amplex Red Assay kit (#A22188, Thermo Fisher). Fluorescence was measured using a microplate reader (Bio-Tek) with Gen5 software at 37°C.

2.12. Estrogen measurement ELISA

Estrogen levels in the mouse AH after IP injection of cyclodextrin-encapsulated 17β-estradiol were measured using Estradiol ELISA kit (ab108667, Abcam). AH was collected as described previously and a colorimetric readout of the estrogen concentration was recorded using a microplate reader (Bio-Tek) with Gen5 software.

2.13. Estrogen metabolite analysis

Normal and FECD human tissues or corneal cups dissected from mice euthanized at week 4 post-UVA were collected and stored at – 80°C. Two pooled mouse corneal cups (same-sex and treatment) or human tissues (pooled as described in the Results section) were snap frozen in liquid nitrogen, mechanically ground, and subjected to solvent extraction with methanol/water (1:1) three times. Supernatant fractions were pooled, concentrated using Speed-Vac, and lyophilized. The lyophilized residue was resuspended in 70 μl of methanol/water 1:1 with 0.1 % formic acid and filtered through a 5000-molecular weight cutoff filter (Millipore) before analysis by ultraperformance liquid chromatography/tandem mass spectrometry (UPLC/MS/MS). The details of sample analysis on UPLC/MS/MS were described in earlier studies [7,44]. The levels of metabolites in the mouse samples were normalized to the weight of the corneal cups, while those in the human specimens were normalized to the DNA concentration determined from the pellet using QIAamp DNA mini kit (#51304, Qiagen, USA) and a PicoGreen kit (#P7589, Thermo Fisher, USA) for DNA extraction and quantification respectively.

2.14. Mitochondrial fragmentation analysis

After stressing with UVA and E2-biotin, the cells were stained with Tom20 antibody to visualize the mitochondrial morphology. The captured images were imported in ImageJ and mitochondrial fragmentation count (MFC) was calculated by counting non-contiguous mitochondrial particles and dividing by the number of pixels which comprise the mitochondrial network i.e., the total number of objects/sums of all object voxels X 100 per cell. The values were exported to Excel for statistical analysis.

2.15. Statistical analysis

We performed Student's *t*-test (Unpaired) for two groups and One-way ANOVA (Tukey's multiple comparison test) or Brown-Forsythe ANOVA (Dunnett's T3 multiple comparisons test) for more than two groups, using GraphPad Prism 8 (V8, La Jolla, CA). The level of significance was chosen at *p < 0.05, **p < 0.01, ***p < 0.001, ****p < 0.0001. Data are expressed as mean ± standard error of mean (SEM) with 95 % confidence interval (unless otherwise specified). All experiments were repeated thrice using 3 to 6 technical replicates each time.

3. Results

3.1. Human corneal tissue and aqueous humor show increased CYP1B1-mediated estrogen-DNA adducts

Previous studies have shown upregulation of CYP1B1 protein in human cornea [7]. To investigate the contribution of CYP1B1 in FECD, we analyzed estrogen metabolites in normal and FECD human tissues containing EDM as well as aqueous humor using a mass spectrometer (UPLC/MS/MS). Table 1 shows all the relevant biological information about the tissues. Tissues from four FECD donors were pooled to achieve one sample (n) to compensate for the low cell count of a single diseased tissue, while tissues from normal donors were not pooled and used individually. In the aqueous humor, 4-hydroxyestradiol (4-$OHE_{1/2}$), a potentially toxic CYP1B1-mediated metabolite, was significantly increased (2-fold) in FECD compared to normal controls (Fig. 1c). Similarly, in FECD EDM tissues, estrogen DNA adducts (4-$OHE_{1/2}$DNA adduct) were significantly increased (6-fold) compared to normal controls (Fig. 1d). Additionally, non-toxic, protective 4-$OCH_3E_{1/2}$ (4-COMT) conjugates were significantly decreased (20-fold) in FECD compared to normal EDM tissues (Fig. 1e). This could be due to the previously detected loss of the enzyme catechol-O-methyltransferase (COMT) in FECD; COMT is known to methylate catechol estrogens to form nontoxic catechol conjugates without ROS generation [30]. This metabolite data suggests that the estrogen genotoxic pathway is upregulated with a concomitant downregulation of the non-toxic protective pathways in FECD patients. Since FECD is highly prevalent in females, we analyzed male and female differences in the estrogen metabolites for FECD. There was no difference in the levels of 4-$OHE_{1/2}$ in the aqueous humor (Supplemental Fig. 1a) or 4-$OHE_{1/2}$ DNA adducts in the EDM tissue (Supplemental Fig. 1b) between males and females in both normal and FECD groups; indicating that both males and females harbor metabolite-driven changes after the onset of degeneration. Of note, there were greater levels of 4-COMT conjugates in normal females compared to males and FECD females, indicating that the generation of protective catechol estrogens is deficient in FECD (Supplemental Fig. 1c). With respect to non-toxic CYP1A1-related metabolites, there were no significant differences for 2-hydroxyestradiol (2-$OHE_{1/2}$) in the aqueous humor (Supplemental Figs. 1d and e) or 2-$OHE_{1/2}$DNA adducts (Supplemental Fig f, g) and 2-$OCH_3E_{1/2}$ (2-COMT) conjugates in EDM tissues (Supplemental Fig h, i) between normal and FECD or males and females.

Since CYP1B1 and its associated metabolites as well as adducts were significantly higher in FECD, we also investigated CYP1B1 induction by its pharmacological activator 2,3,7,8-tetrachlorodibenzo-p-dioxin (TCDD). We found that CYP1B1 was increased in normal female (SVN1-67F) (6.3-fold), FECD female (SVF1-73F) (4.5-fold), and FECD male (SVF3-76M) (4.5-fold) cell lines in response to TCDD with no changes in a normal male (SVN3-65M) cell line (Fig. 1f and g). This suggests that the estrogen metabolizing enzyme CYP1B1 is highly inducible in FECD female and male cell lines irrespective of sex. Previously we have shown mtDNA damage and CYP1B1 translocation to the mitochondria after UVA-induced Fuchs dystrophy [7]. Since FECD specimens showed increased estrogen metabolite formation and greater mtDNA damage [22], we investigated whether estrogen translocated to

mitochondria and provided the substrate for the CYP1B1-mediated estrogen metabolism in human specimens. Using immunohistochemistry and confocal microscopy, we detected colocalization of estrogen using E2-biotin within mitochondria of CEnCs in the FECD specimens (Fig. 1h), indicating that estrogen is a possible substrate for mitochondrial CYP1B1.

3.2. UVA irradiation causes the greatest CEnC loss and FECD phenotype in *Nqo1*$^{-/-}$ females

Previously, we showed a decrease in a key antioxidant protein, NQO1, in the *ex vivo* FECD tissue [30] and FECD cell lines [30] leading to the oxidant-antioxidant imbalance seen in FECD. We also demonstrated increased estrogen-DNA adducts in an *NQO1*$^{-/-}$ CEnC cell line in response to oxidative stress [30]; however, *in vivo* data was lacking. Hence, we generated the *Nqo1*$^{-/-}$ mice and irradiated *Nqo1*$^{+/+}$ and *Nqo1*$^{-/-}$ (male and female) with 500 J/cm^2 UVA, which was the dose that showed the most discernible differences between the sexes previously (Fig. 2a) [7]. We confirmed the *Nqo1*$^{-/-}$ mice genotype by PCR (Fig. 2b) and Western blot (Fig. 3a) analyses and further characterized *Nqo1*$^{-/-}$ mice to ensure lack of ocular developmental defects. *Nqo1*$^{-/-}$ mice were normal in appearance compared to *Nqo1*$^{+/+}$ with no phenotypic differences in the eye prior to irradiation.

Since extracellular matrix deposition and CEnC junctional changes are a hallmark of FECD, we evaluated Descemet's membrane (DM) thickness using hematoxylin and eosin (H&E) and periodic acid-schiff (PAS) staining and characterized CEnC morphology using Zonula occludens-1 (ZO-1) staining. The CEnC number was quantified by using HRT at pre-UVA as well as weeks 2 and 4 post-UVA. UVA irradiation caused an epithelial defect and corneal swelling at day 1 in all genotypes, including *Nqo1*$^{-/-}$ females, which demonstrated immediate swelling of the cornea at day 1 post-UVA, as shown in the representative image (Fig. 2c). Compared to *Nqo1*$^{+/+}$ there was an increase in DM thickness shown by H&E and PAS staining (Fig. 2d and e) and loss of junctional contacts shown by ZO-1 staining leading to enlarged irregular CEnCs (Fig. 2f) in *Nqo1*$^{-/-}$ at week 4 post-UVA.

The *in vivo* HRT analysis revealed no significant difference in the CEnC number between the genotypes and sexes before UVA (Supplemental Fig. 2a), suggesting that loss of NQO1 did not affect CE cell number during development. At week 1 post-UVA, there was a significant decrease in CEnC number in *Nqo1*$^{+/+}$ female (23 %), *Nqo1*$^{-/-}$ male (25 %), *Nqo1*$^{-/-}$ female (35.3 %) but not in *Nqo1*$^{+/+}$ male mice (8.5 %) compared to CEnC number pre-UVA, indicating that *Nqo1*$^{-/-}$ females were most sensitive to cell loss at early time-points (Fig. 2h, Supplemental Fig. 2b). At week 2 post-UVA, *Nqo1*$^{-/-}$ female had the most significant decrease (45.2 %) in CEnC number, while *Nqo1*$^{-/-}$ male and *Nqo1*$^{+/+}$ female had an equal decrease in CEnC number (24 %) followed by *Nqo1*$^{+/+}$ male (8.5 %) compared to CEnC number pre-UVA (Fig. 2h and i), indicating that a continuous and rapid decline in cell loss persisted in *Nqo1*$^{-/-}$ females, differentiating them from the other cohorts. Interestingly, there was similar cell loss between *Nqo1*$^{+/+}$ females and *Nqo1*$^{-/-}$ males at this time-point, suggesting that NQO1 depletion in males provides the same effect as baseline hormone (i.e. estrogen metabolite)-mediated genotoxicity seen in wild type females [7]. The loss of NQO1 in females showed maximum susceptibly, which was further evident at 4 weeks post UVA, where *Nqo1*$^{-/-}$ females had a 59.9 % decrease in CEnCs, while *Nqo1*$^{+/+}$ female, *Nqo1*$^{-/-}$ male, and *Nqo1*$^{+/+}$ male had a 41.2 %, 23.4 %, and 16.1 % decrease, respectively, compared to pre-UVA (Fig. 2 h, j). This was a critical time point where CEnC loss in *Nqo1*$^{+/+}$ females exceeded that of *Nqo1*$^{-/-}$ males, indicating the female sex was a predominant factor in CEnC susceptibility to degenerative loss. The finding of greatest and continuous cell loss in *Nqo1*$^{-/-}$ females suggests the absence of NQO1 activity has an augmented effect on the CEnC loss in females, the mechanism of which is further investigated below. Of note, there were no significant differences in CCT at weeks 1, 2, and 4 post-UVA compared to baseline CCT (pre-UVA) across all genotypes (Supplemental Fig. 2c), suggesting that this particular dose of UVA, although sufficient to cause CEnC damage, was not high enough to induce corneal edema, unlike seen with 1000 J/cm^2 UVA dose [7].

3.3. CYP1B1-metabolizing estrogen metabolites and adducts are increased in *Nqo1*$^{-/-}$ female mice post-UVA

CYP1B1 drives the conversion of $E_{1/2}$ into 4-$OHE_{1/2}$ followed by the generation of reactive catechol quinones which generate ROS [45,46] and toxic depurinating estrogen DNA adducts (4-$OHE_{1/2}$ adducts) [47] (Fig. 1b). In the current study, UVA decreased NQO1 protein levels (1.27-fold) in *Nqo1*$^{+/+}$ female mice (Fig. 3a and b), with a similar decrease in *Nqo1*$^{+/+}$ male mice (Sup Fig. 3e) at day 1 post-UVA. Similarly, UVA significantly increased CYP1B1 protein expression (4.0-fold) in *Nqo1*$^{-/-}$ female mice compared to *Nqo1*$^{+/+}$ females. Although UVA did not upregulate COMT, known to generate protective catechol conjugates (Fig. 1b), in *Nqo1*$^{+/+}$ females, there was a significant decrease in COMT levels (3-fold) in *Nqo1*$^{-/-}$ females compared to non-UVA control (Fig. 3a and d). UVA irradiation also increased ROS levels in the aqueous humor of *Nqo1*$^{-/-}$ female mice compared to *Nqo1*$^{+/+}$ female, *Nqo1*$^{+/+}$ male, and *Nqo1*$^{-/-}$ male mice respectively (1.7, 2.2, 2.6-fold), at week 4 (Fig. 3e). Analysis of estrogen metabolites by UPLC/MS/MS showed a significant increase of toxic CYP1B1-related 4-$OHE_{1/2}$ (4-fold, $p < 0.0005$) and 4-$OHE_{1/2}$ DNA adducts (50-fold, $p < 0.0001$) in EDM complexes of *Nqo1*$^{+/+}$ female mice compared to *Nqo1*$^{-/-}$ male, *Nqo1*$^{+/+}$ male, and *Nqo1*$^{+/+}$ female mice at week 4 post-UVA (Fig. 3f and g). There was also a trend towards increased 4-quinone conjugates in *Nqo1*$^{-/-}$ female mice compared to *Nqo1*$^{+/+}$ female mice (Supplemental Fig. 3d), which ultimately contributes to estrogen-DNA adducts [47]. Interestingly, the non-harmful 4-$OCH_3E_{1/2}$ (4-COMT conjugates) significantly decreased (4.3-fold, $p < 0.05$) in *Nqo1*$^{-/-}$ females compared to *Nqo1*$^{+/+}$ females (Fig. 3h), similar to the findings in FECD human specimens (Fig. 1e), suggesting that lack of COMT upregulation in *Nqo1*$^{-/-}$ females leads to decreased levels of protective methoxy estrogen conjugates that are generated when estrogen quinones are reduced back to catechol estrogens by NQO1. Therefore, when NQO1 is lost, UVA leads to a more robust production of ROS that is compounded by lack of catechol quinone neutralization and continuous conversion of 4-$OHE_{1/2}$ to harmful 4-$OHE_{1/2}$ adducts, thus accelerating the estrogen genotoxic pathway.

CYP1A1 is another estrogen metabolizing enzyme, which converts $E_{1/2}$ to 2-$OHE_{1/2}$, followed by the generation of 2-$OHE_{1/2}$ DNA adducts, that are less likely to cause DNA mutations and cellular toxicity compared to CYP1B1 metabolites [48]. *Nqo1*$^{-/-}$ females also showed a 20-fold increase in 2-$OHE_{1/2}$ compared to *Nqo1*$^{+/+}$ and *Nqo1*$^{-/-}$ males and a 1.33-fold significant increase compared to *Nqo1*$^{+/+}$ females at week 4 post-UVA (Supplemental Fig. 3a). However, 2-$OHE_{1/2}$ DNA adducts significantly decreased (3.5-fold) in *Nqo1*$^{-/-}$ females compared to *Nqo1*$^{-/-}$ males (Supplemental Fig. 3b), suggesting that even though 2-$OHE_{1/2}$ metabolites were high, they did not lead to the formation of 2-$OHE_{1/2}$ DNA adducts. Similarly, 2-$OCH_3E_{1/2}$ significantly decreased (2-fold) in *Nqo1*$^{-/-}$ females compared to *Nqo1*$^{-/-}$ males (Supplemental Fig. 3c). Overall, there was a similar trend between CYP1A1-and CYP1B1-mediated metabolites in *Nqo1*$^{-/-}$ females compared to other genotypes, except for 2-$OHE_{1/2}$ DNA adducts. Taken together, these data suggest that loss of NQO1 amplifies the estrogen genotoxic pathway in females as evidenced by the increased CYP1B1-derived estrogen metabolites and DNA-adducts along with decreased non-toxic catechol conjugates. This likely contributes to redox imbalance resulting in the greatest CEnC loss in *Nqo1*$^{-/-}$ females compared to other genotypes and renders female mice the most susceptible to CEnC loss post UVA. (Fig. 3i).

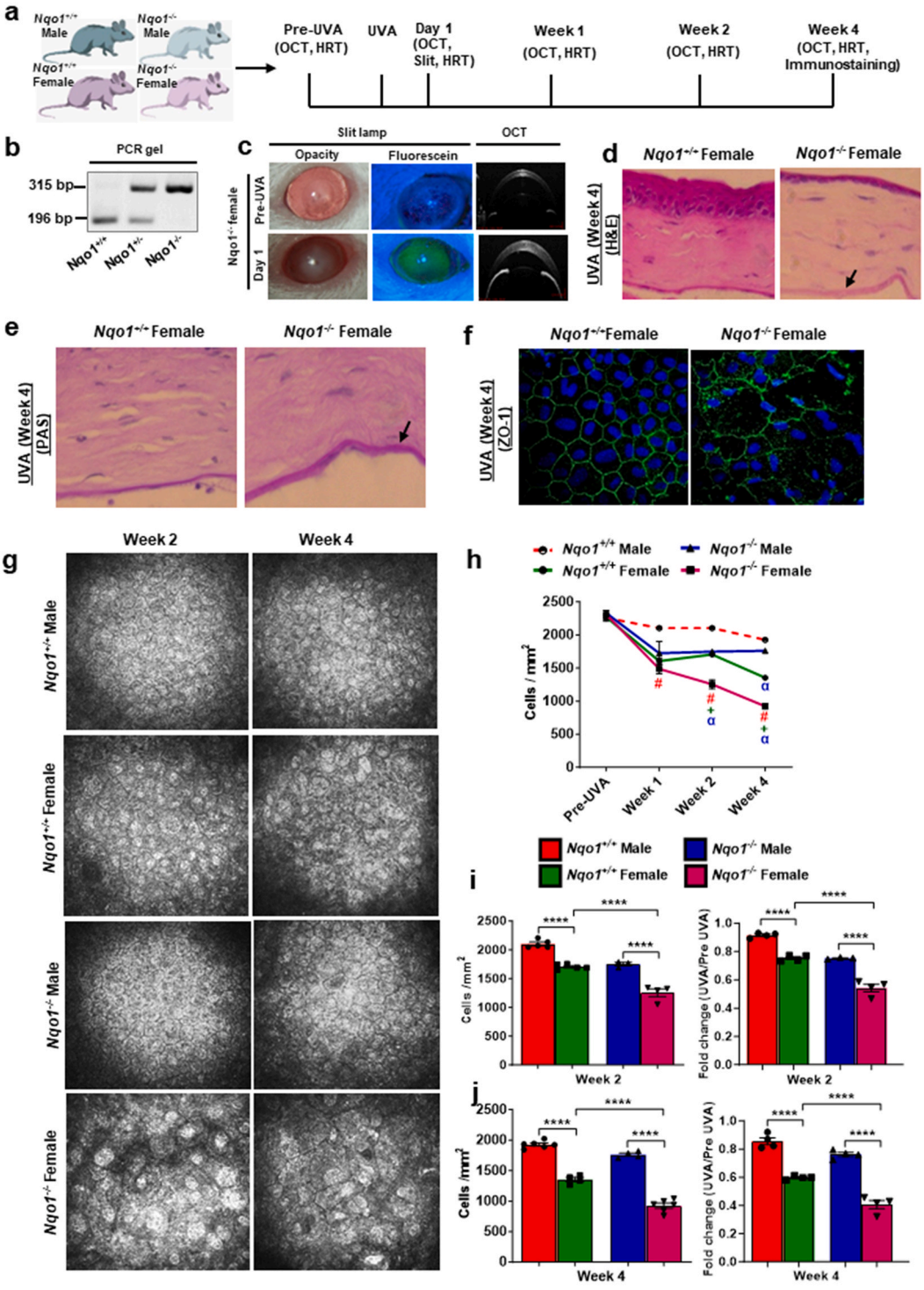

Fig. 2. *Nqo1*$^{-/-}$ female mice are most susceptible to loss of CEnCs after UVA treatment. (a) Timeline for evaluation of various phenotypic parameters in *Nqo1*$^{+/+}$ and *Nqo1*$^{-/-}$ male and female mice post-UVA treatment. (b) Genotyping PCR gel confirming the homozygous knockout of NQO1 in *Nqo1*$^{-/-}$ mice. (c) Corneal opacity and epithelial defect assessed by slit lamp exam using white and blue light illumination with fluorescein staining (green) respectively, and corneal swelling measured by OCT at day 1 post-UVA in *Nqo1*$^{-/-}$ female mice. Descemet's membrane (DM) thickening indicated by the arrow in *Nqo1*$^{-/-}$ female mice at week 4 post-UVA using (d) hematoxylin and eosin (H&E) staining and (e) periodic acid-schiff (PAS) staining. (f) Zonula occludens-1 (ZO-1, green) immunostaining showing enlargement and loss of corneal endothelial (CE) cells in *Nqo1*$^{-/-}$ female at week 4 post-UVA. (g) *In vivo* confocal HRT images of *Nqo1*$^{+/+}$ and *Nqo1*$^{-/-}$ male and female mice at week 2 and 4 post-UVA (Scale bar: 100 μm). (h, i, j) Comparison of CEnC numbers in *Nqo1*$^{+/+}$ and *Nqo1*$^{-/-}$ male and female mice pre-UVA and at week 1,2 and 4 post-UVA (n = 4, *p < 0.05). #, +, and α, represent significant differences between *Nqo1*$^{-/-}$ females and *Nqo1*$^{+/+}$ *males, Nqo1*$^{+/+}$ females, and *Nqo1*$^{-/-}$ males respectively.

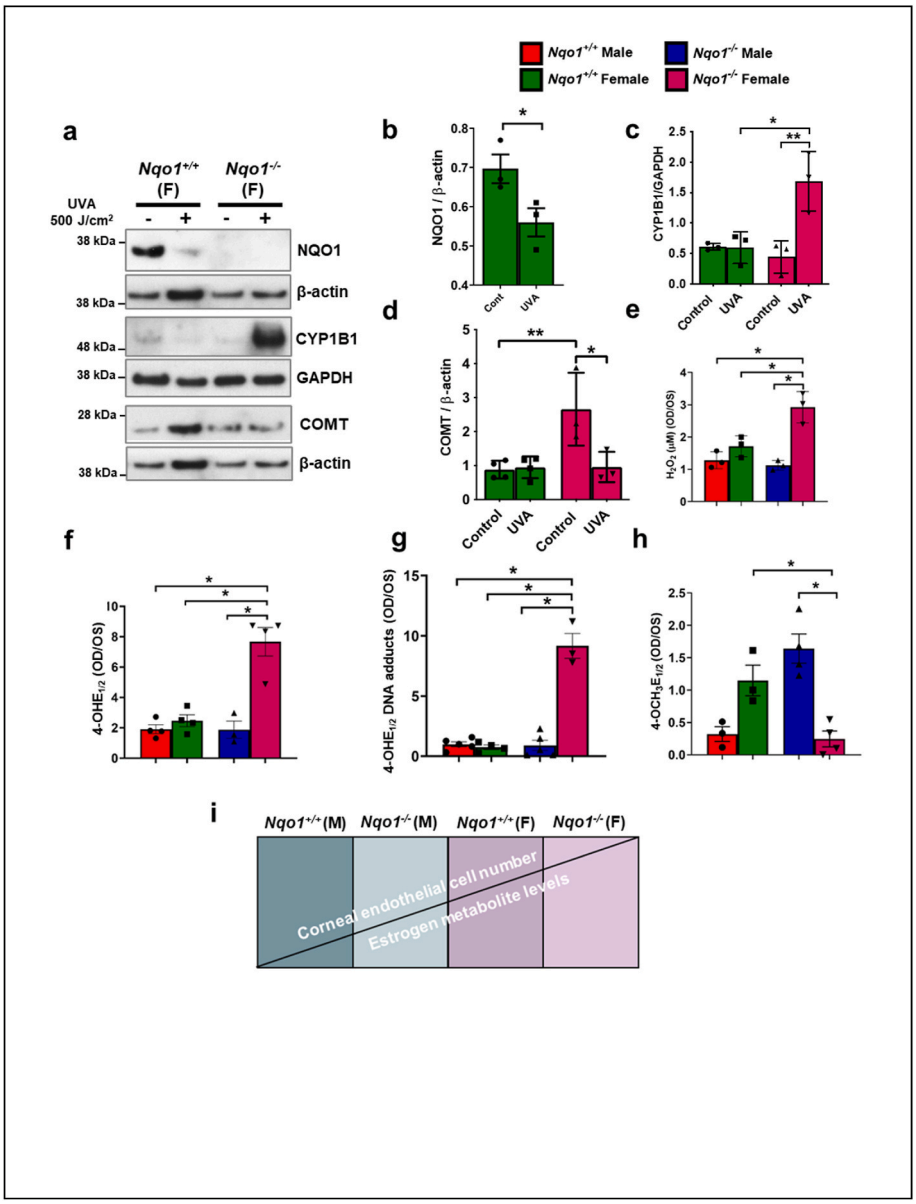

Fig. 3. CYP1B1-related toxic metabolites are upregulated, and antioxidant protein NQO1 and non-toxic catechol conjugates are downregulated in *Nqo1*$^{-/-}$ female mice after UVA treatment. (a) Representative western blots of NQO1, CYP1B1, and COMT, and densitometry showing (b) downregulation of NQO1 in *Nqo1*$^{+/+}$ females, (c) increased CYP1B1, and (d) downregulated protective enzyme COMT in *Nqo1*$^{-/-}$ compared to *Nqo1*$^{+/+}$ females at day 1 post-UVA irradiation. (e) Upregulation of reactive oxygen species (ROS) at day 1 and an increase in CYP1B1-mediated harmful metabolites, namely (f) catechol estrogens (4-$OHE_{1/2}$) and (g) estrogen DNA adducts (4-$OHE_{1/2}$-DNA adducts) along with downregulation of (h) COMT-mediated protective catechol conjugates (4-$OCH_3E_{1/2}$) at week 4 post-UVA irradiation in *Nqo1*$^{-/-}$ females compared to *Nqo1*$^{-/-}$ males and *Nqo1*$^{+/+}$ -males and -females (n = 4, *p < 0.05) (i) Diagram showing the inverse relationship between levels of CYP1B1-mediated estrogen metabolites and CEnC count, indicating that cell loss is inversely associated with harmful estrogen metabolites seen due to the lack of neutralizing effect of NQO1.

3.4. TMS and berberine attenuates CEnC loss after UVA

To determine whether CYP1B1 activation causes CEnC loss in *Nqo1*$^{-/-}$ females, we used a systemic administration of a specific CYP1B1 inhibitor, TMS, right after UVA irradiation in *Nqo1*$^{+/+}$ and *Nqo1*$^{-/-}$ female mice (Fig. 4a). There was no significant difference in CEnC number at the baseline between vehicle (DMSO)- and TMS-treated *Nqo1*$^{+/+}$ and *Nqo1*$^{-/-}$ female groups (Fig. 4c, Sup Fig. 4a). At week 2 post-UVA, there was a 37.6 % CEnC loss in the DMSO-treated *Nqo1*$^{+/+}$ female mice, 19.2 % CEnC loss in the TMS-treated *Nqo1*$^{+/+}$ female mice, 42.1 % CEnC loss in the DMSO-treated *Nqo1*$^{-/-}$ female mice, and 27.9 % CEnC loss in the TMS-treated *Nqo1*$^{-/-}$ female mice compared to their respective pre-UVA baseline (Fig. 4b, c, d). Thus, at week 2 post-UVA, TMS-treated *Nqo1*$^{+/+}$ female mice showed an 18.4 % CEnC rescue compared to DMSO-treated *Nqo1*$^{+/+}$ females, and TMS-treated *Nqo1*$^{-/-}$ female showed a 14.2 % CEnC rescue compared to DMSO-treated *Nqo1*$^{-/-}$ females. Similarly, at week 4 post-UVA, there was a 51 % CEnC loss in the DMSO-treated *Nqo1*$^{+/+}$ female mice, 37.6 % CEnC loss in the TMS-treated *Nqo1*$^{+/+}$ female mice, 54 % CEnC in the DMSO-treated *Nqo1*$^{-/-}$ female mice, and 41.8 % CEnC loss in the TMS-treated *Nqo1*$^{-/-}$ female mice compared to their respective pre-UVA baseline (Fig. 4b, c, d). Thus, at week 4 post-UVA, TMS-treated *Nqo1*$^{+/+}$ females showed a 13.4 % CEnC rescue compared to DMSO-treated *Nqo1*$^{+/+}$ females while TMS-treated *Nqo1*$^{-/-}$ females showed a 12.2 % CEnC rescue compared to DMSO-treated *Nqo1*$^{-/-}$ females. We also compared the effect of TMS on the rescue of CEnC loss between the

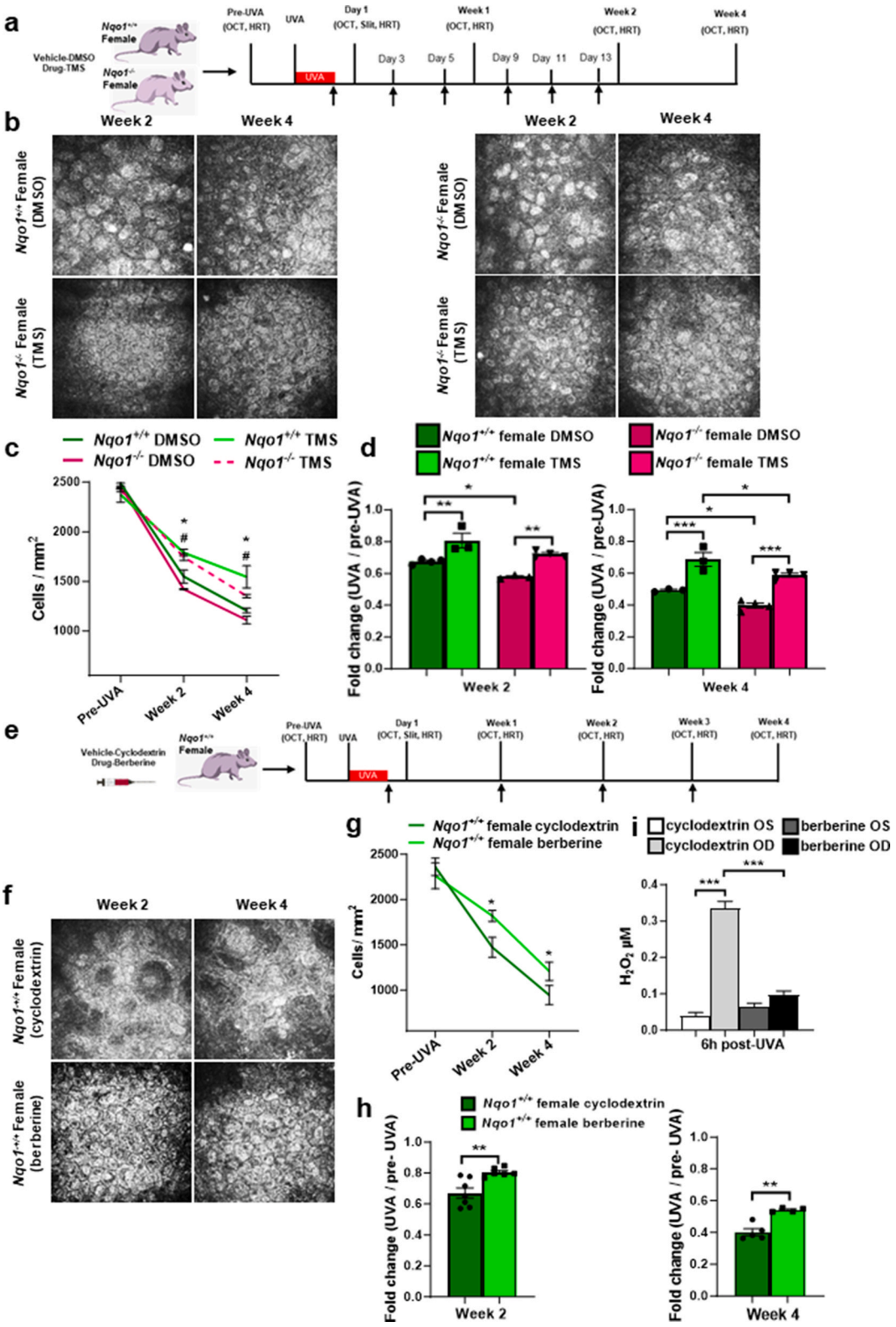

Fig. 4. CYP1B1-specific inhibitor TMS prevents CEnC loss in *Nqo1*$^{+/+}$ and *Nqo1*$^{-/-}$ females, and antioxidant as well as CYP1B1 inhibitor, berberine, rescues CEnC loss and prevents ROS formation in *Nqo1*$^{+/+}$ females post-UVA. (a) Schematic of the treatment regimen of TMS indicated by black arrows. (b) *In vivo* confocal HRT images of vehicle (DMSO)- or TMS-treated *Nqo1*$^{+/+}$ and *Nqo1*$^{-/-}$ female mice at weeks 2 and 4 post-UVA. (c, d) Quantification of CEnC number and fold change from baseline at weeks 2 and 4 post-UVA (n = 4, *p < 0.05; * or # represents significance for TMS-treated *Nqo1*$^{+/+}$ or *Nqo1*$^{-/-}$ females compared to DMSO-treated *Nqo1*$^{+/+}$ or *Nqo1*$^{-/-}$ females respectively). (e) Schematic of the treatment regimen of berberine indicated by black arrows. (f) *In vivo* confocal HRT images of vehicle (cyclodextrin)- or berberine-treated *Nqo1*$^{+/+}$ female mice at weeks 2 and 4 post-UVA. (g, h) Quantification of CEnC number and fold change from baseline at weeks 2 and 4 post-UVA (n = 5, *p < 0.05, **p < 0.01). (i) ROS measured as H_2O_2 levels in the aqueous humor from UVA-exposed (OD) and non-exposed control (OS) eyes of berberine-treated compared to cyclodextrin-treated *Nqo1*$^{+/+}$ female mice (n = 4, ***p < 0.001) at 6 h post-UVA.

two genotypes (*Nqo1*$^{+/+}$ and *Nqo1*$^{-/-}$ females) at weeks 2 and 4 post-UVA. TMS-treated *Nqo1*$^{+/+}$ female mice had 1.19- and 1.38-fold higher CEnC number, while TMS-treated *Nqo1*$^{-/-}$ female mice had 1.26- and 1.49-fold higher CEnC number, at weeks 2 and 4 post-UVA compared to DMSO-treated *Nqo1*$^{+/+}$ and *Nqo1*$^{-/-}$ mice respectively (Fig. 4d). However, CEnC rescue was 1.4-fold more in TMS-treated *Nqo1*$^{+/+}$ compared to TMS-treated *Nqo1*$^{-/-}$ at week 4 only, and not at week 2, post-UVA (Fig. 4d). This rescue was specific to female mice, as TMS did not significantly rescue CEnCs in *Nqo1*$^{+/+}$ and *Nqo1*$^{-/-}$ male mice post UVA (Supplemental Fig. 5), prompting the studies on estrogen injection in male mice. As expected, TMS did not influence the rescue of CCT, as the current dose of UVA did not cause corneal edema (Supplemental Fig. 4b).

Since NQO1 is downregulated while CYP1B1 is upregulated in FECD specimens, we investigated the effect of a naturally occurring compound, berberine (known to have both NRF2-NQO1 induction and CYP1B1 inhibition properties) [49,50] on CEnC loss in *Nqo1*$^{+/+}$ female mice (Fig. 4e). At week 2 post-UVA, there was a 37.5 % CEnC loss in the vehicle (cyclodextrin)-treated group and only a 19.5 % CEnC loss in the berberine-treated group compared to their respective pre-UVA baseline. (Fig. 4f and g). Thus, at week 2 post-UVA, berberine-treated *Nqo1*$^{+/+}$ females demonstrated an 18 % CEnC rescue and 1.2-fold higher CEnC number compared to the cyclodextrin-treated *Nqo1*$^{+/+}$ females (Fig. 4g and h). At week 4 post-UVA, there was a 59 % CEnC loss in the cyclodextrin-treated group and a 46.5 % CEnC loss in the berberine-treated group compared to their respective pre-UVA baseline (Fig. 4f and g). Thus, at week 4 post-UVA, berberine-treated *Nqo1*$^{+/+}$ females demonstrated a 12.6 % CEnC rescue, however, had 1.3-fold higher CEnC number compared to the cyclodextrin-treated *Nqo1*$^{+/+}$ females, indicating that berberine treatment slowed the rate of cell loss from week 2 to week 4 post-UVA (Fig. 4h). The investigation of ROS production in the aqueous humor in response to UVA-irradiation revealed significant increase of H_2O_2 levels (8.2-fold; OD/OS) in the cyclodextrin-treated mice. However, the H_2O_2 production was significantly inhibited in berberine-treated mice with their OD eyes having 72 % lower H_2O_2 than cyclodextrin-treated mice at 6 h post-UVA, thus demonstrating the antioxidant effect of berberine (Fig. 4i).

3.5. Estrogen treatment increases CEnC loss and CYP1B1-mediated 4-OHE$_{1/2}$ estrogen DNA adducts in *Cyp1b1*$^{+/+}$ but not in *Cyp1b1*$^{-/-}$ male mice

To investigate the direct role of estrogen in CYP1B1-mediated genotoxicity, we performed systemic injections (IP) of E2 in *Cyp1b1*$^{+/+}$ and *Cyp1b1*$^{-/-}$ male mice after UVA irradiation, as previously described [40] (Fig. 5a). Interestingly, E2-treated *Cyp1b1*$^{+/+}$ male mice had a 40.5 and 60.1 % CEnC loss, which was 26.7 % and 40 % more than (non-E2-treated) *Cyp1b1*$^{+/+}$ male mice at 2- and 4-weeks post-UVA, respectively. Estrogen injections caused a decline in CEnC number in males to a similar level of cell loss seen in *Nqo1*$^{-/-}$ females, validating the estrogen-induced endothelial toxicity model. However, the E2-treated *Cyp1b1*$^{-/-}$ male mice had only 23.5 % and 36.3 % CEnC loss at 2- and 4-weeks post-UVA respectively, compared to the pre-UVA levels. Thus, *Cyp1b1*$^{-/-}$ male mice showed a 17 % and 23.8 % CEnC rescue at 2 and 4 weeks, respectively, compared to *Cyp1b1*$^{+/+}$ at similar time points post-UVA (Fig. 5b and c). Similar results were obtained for E2-treated *Cyp1b1*$^{+/+}$ (30.9 %, 50.5 % decrease in CEnC number) and *Cyp1b1*$^{-/-}$ mice (17.2 %, 25.9 % decrease in CEnC number) compared to their respective non-E2-treated groups at weeks 2 and 4, respectively, post-UVA. (Fig. 5b and c). Corneal thickness was not affected by estrogen injections after UVA or by CYP1B1 loss, similar to *Nqo1*$^{-/-}$ data. (Supplemental Fig. 7b). In summary, the absence of CYP1B1 mitigated the estrogen induced CEnC loss seen in male mice after UVA.

To determine estrogen bioavailability in the corneal endothelium after systemic administration, we quantified the levels of E2 in the anterior chamber (AC) fluid of *Cyp1b1*$^{+/+}$ and *Cyp1b1*$^{-/-}$ male mice. There was a 1500-fold increase in E2 in estrogen-treated compared to vehicle-treated *Cyp1b1*$^{+/+}$ and *Cyp1b1*$^{-/-}$ mice at 2 h post-UVA (Fig. 5d), indicating a similar AC distribution of estrogen after systemic administration. To determine the effect of estrogen metabolism on CEnC loss, endothelial metabolites were assayed in corneal endothelial cell samples of E2-treated *Cyp1b1*$^{+/+}$ and *Cyp1b1*$^{-/-}$ male mice. Estrogen injection led to significant upregulation (3- and 4-fold) of 4-OHE$_{1/2}$ and DNA adducts in *Cyp1b1*$^{+/+}$ male mice after UVA, to the levels seen in *Nqo1*$^{-/-}$ female mice. However, E2-treated *Cyp1b1*$^{-/-}$ male mice showed a significant downregulation of 4-OHE$_{1/2}$ (150-fold) and 4-OHE$_{1/2}$ adducts (1.85-fold) compared to *Cyp1b1*$^{+/+}$ males at week 4 post-UVA and estrogen treatment (Fig. 5e). Non-toxic 4-OCH$_3$E$_{1/2}$ catechol conjugates also significantly increased (110-fold) in *Cyp1b1*$^{-/-}$ mice compared to CYP1B1+/+ at week 4 post-UVA (Fig. 5e). Interestingly, we found that CYP1A1-mediated 2-OCHE$_{1/2}$ metabolites and DNA adducts significantly decreased in *Cyp1b1*$^{-/-}$ male mice compared to *Cyp1b1*$^{+/+}$ mice at week 4 post-UVA and estrogen treatment, suggesting a potential overlapping function between both enzymes (Supplemental Fig. 7c). However, there was no significant difference in 4-OCH$_3$E$_{1/2}$ in *Cyp1b1*$^{+/+}$ and *Cyp1b1*$^{-/-}$ mice at week 4 post-UVA and estrogen (Supplemental Fig. 7d). In summary, this data suggests that cell loss rescue seen in CYP1B1-null mice is likely due to a lack of harmful estrogen metabolite production seen in estrogen-treated male mice. Decreased CYP1B1-mediated metabolites and adducts (4-OHE$_{1/2}$) and increased nontoxic catechol conjugates (4-OCH$_3$E$_{1/2}$) after estrogen treatment in *Cyp1b1*$^{-/-}$ male mice post-UVA suggest the absence of CYP1B1 diverted the estrogen breakdown to the protective metabolite formation.

Estrogen translocates to mitochondria in human corneal endothelium cells (Fig. 1h), which can potentially initiate estrogen toxicity and mtDNA damage post-UVA. Since previous studies have shown estrogen metabolite-induced DNA damage in corneal endothelial cells *in vitro* [30], we investigated nDNA and mtDNA damage using LA-qPCR in mouse CEnCs *in vivo*. The relative amplification of the small mtDNA fragment was employed as an estimate of mtDNA copy number and is inversely proportional to mtDNA damage. *Cyp1b1*$^{+/+}$ male mice had 26 % decrease in mtDNA amplification, suggesting increased DNA damage after estrogen treatment compared to vehicle after UVA. However, there was no difference in mtDNA amplification and mtDNA damage between vehicle and estrogen-treated *Cyp1b1*$^{-/-}$ male mice, suggesting that mtDNA damage is mitigated by the deletion of CYP1B1 (Fig. 5f). Similarly, nDNA amplification (*lmpdh* and *Hprt* genes) was decreased, suggesting increased nDNA damage in estrogen-treated *Cyp1b1*$^{+/+}$ and *Cyp1b1*$^{-/-}$ male compared to their respective vehicle (Fig. 5g and h). However, the nDNA damage was not rescued in *Cyp1b1*$^{-/-}$ male mice, unlike mtDNA damage. This data was consistent with a previous study showing that mtDNA damage has been the main differentiating factor in greater female susceptibility to UVA-induced cell loss [7].

3.6. Increased estrogen and UVA-mediated mtDNA genotoxicity and CYP1B1 translocation to mitochondria under complete loss of NQO1 in vitro

To study the effects of estrogen translocation to the mitochondria, we determined mtDNA damage by assessing mitochondrial apurinic/abasic sites using ARP staining after UVA (5 J/cm^2) and estrogen (E2-biotin, 0.3 μM) exposure. To account for any potential non-specific effects of the biotin tag, we treated the cells with an unconjugated, fluorophore 594-labeled biotin alone and noted the absence of staining for the apurinic sites (ARP) (Supplemental Fig. 8a). First, we detected enhanced mitochondrial uptake of estrogen by demonstrating colocalization of E2-biotin within mitochondria labeled with TOM20 antibody after UVA in both *NQO1*$^{+/+}$ (R = 0.73) and *NQO1*$^{-/-}$ (R = 0.8) cells after UVA (Supplemental Fig. 8b). Next, we investigated the effect of UVA on mtDNA damage and morphology, as a surrogate for mitochondrial function (Fig. 6a). At baseline, we did not detect colocalization of ARP

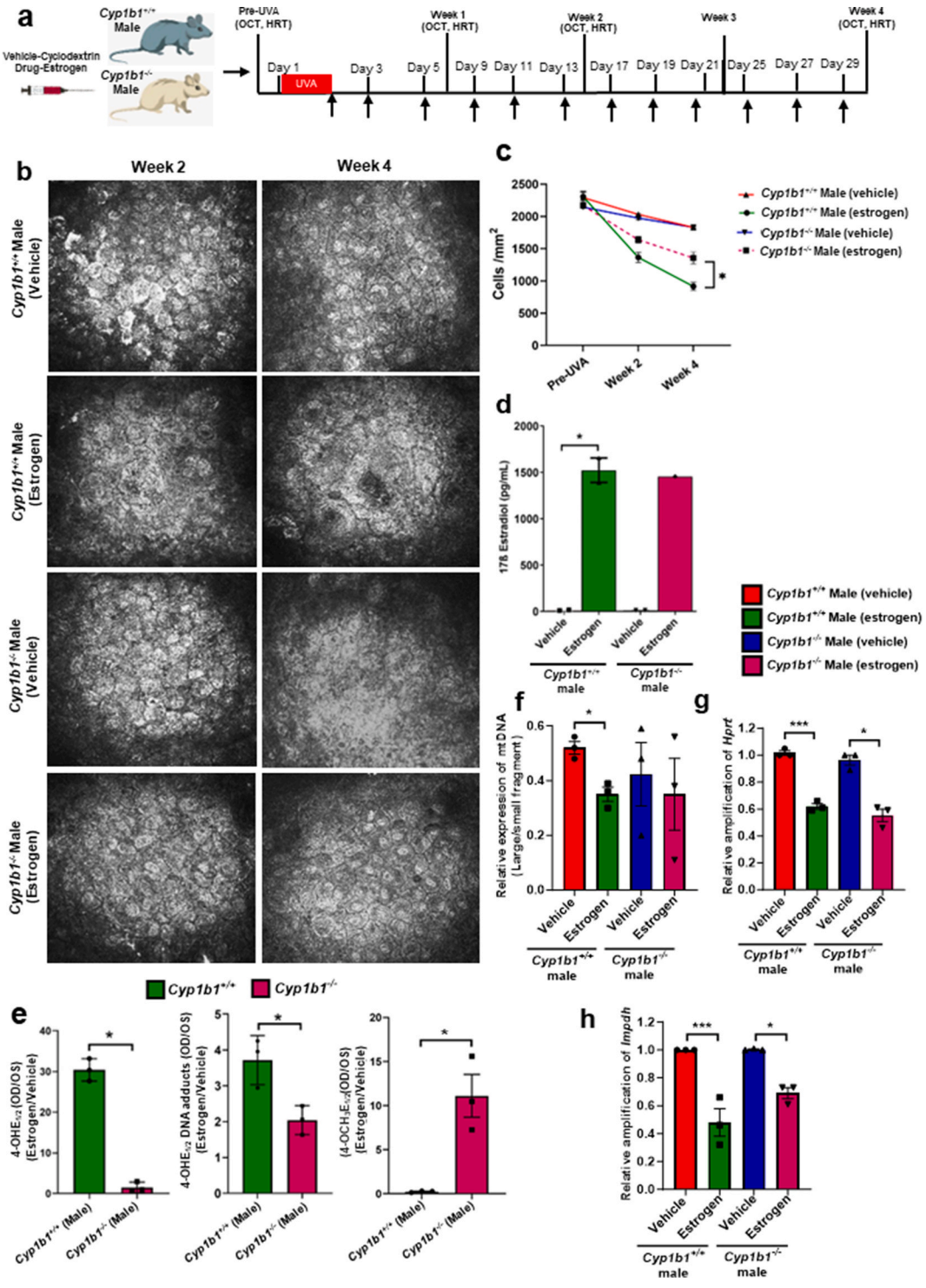

Fig. 5. Estrogen exacerbates CEnC loss and increases CYP1B1-related toxic metabolites and mtDNA damage in *Cyp1b1*$^{+/+}$ but not in *Cyp1b1*$^{-/-}$ male mice after UVA. (a) Schematic diagram for estrogen and cyclodextrin (vehicle) treatment (indicated by black arrow) in *Cyp1b1*$^{+/+}$ and *Cyp1b1*$^{-/-}$ male mice after UVA. (b) *In vivo* confocal HRT images for *Cyp1b1*$^{+/+}$ and *Cyp1b1*$^{-/-}$ male mice treated with vehicle (cyclodextrin) and estrogen (cyclodextrin-encapsulated 17β-estradiol) at week 2 and week 4 post-UVA. (c) Quantification of CEnC numbers in vehicle or estrogen-treated *Cyp1b1*$^{+/+}$ and *Cyp1b1*$^{-/-}$ male mice pre- and week 2 and 4 post-UVA (n = 4, *p < 0.05, where * represents comparison of *Cyp1b1*$^{+/+}$ versus *Cyp1b1*$^{-/-}$ male mice treated with estrogen). (d) Detection of 17β-estradiol in the aqueous humor of *Cyp1b1*$^{+/+}$ and *Cyp1b1*$^{-/-}$ male mice at 2 h post-UVA (n = 3, *p < 0.05). (e) Levels of CYP1B1-related 4-OHE$_{1/2}$, 4-OHE$_{1/2}$-DNA adducts and 4-OCH$_3$E$_{1/2}$ in *Cyp1b1*$^{+/+}$ and *Cyp1b1*$^{-/-}$ male mice at week 4 post-UVA (n = 3, *p < 0.05) (f) Quantification of mtDNA and nuclear (*Hprt, Impdh*) DNA damage using LA-qPCR for *Cyp1b1*$^{+/+}$ and *Cyp1b1*$^{-/-}$ mice at day 1 post-UVA (n = 3, *p < 0.05).

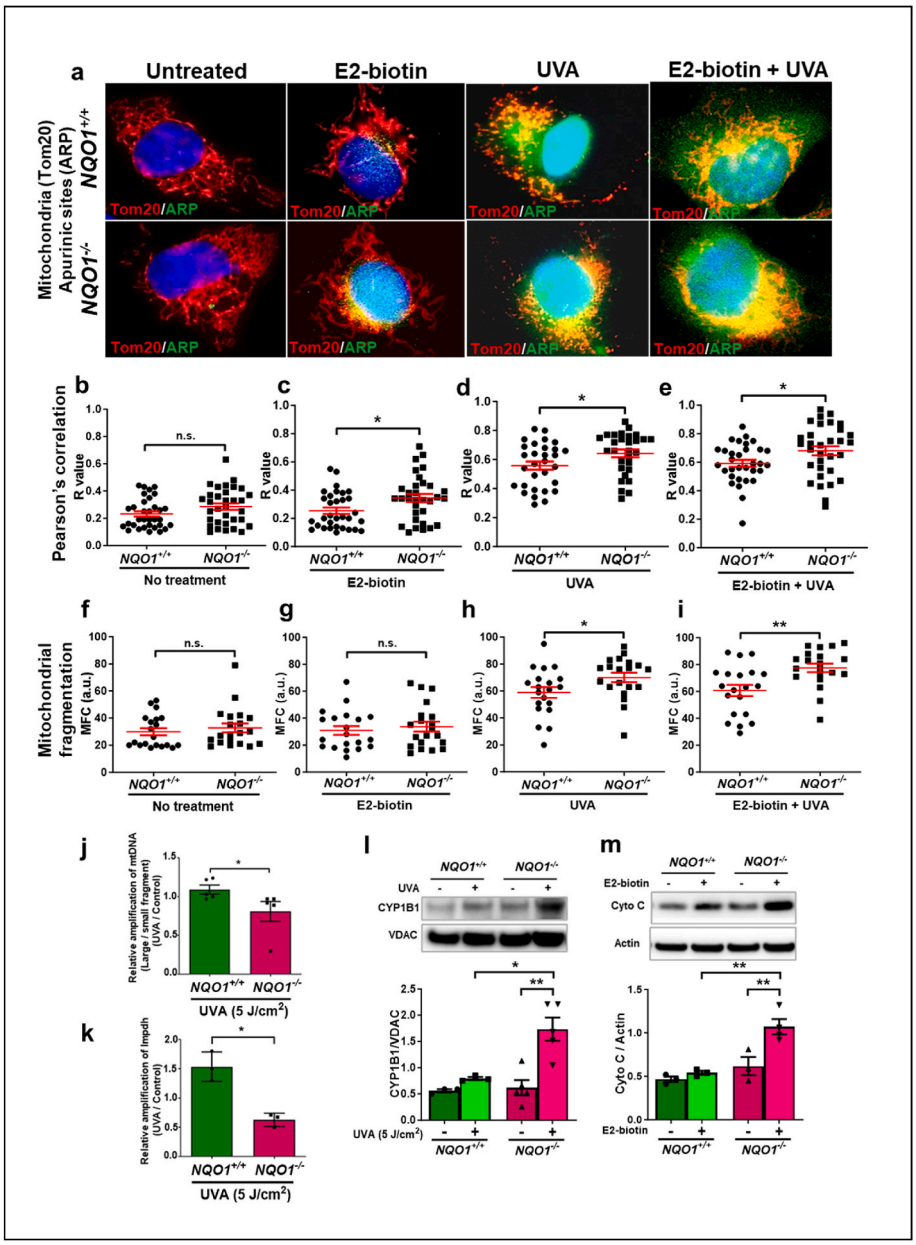

Fig. 6. Estrogen induces mtDNA damage and CYP1B1 translocates to the mitochondria post-UVA in the *Nqo1*$^{-/-}$ cell line. (a) Aldehyde Reactive Probe (ARP, green), co-localized (yellow) with TOM20 (red) in *NQO1*$^{+/+}$ *and NQO1*$^{-/-}$ cells after 6 h of exposure to exogenous estrogen (E2-biotin) alone, UVA alone, or a combination of E2-biotin and UVA. ARP was also detected in the nuclei (DAPI, blue). Co-localization (yellow) of apurinic sites (ARP, green) with mitochondria (TOM20, red) analyzed by R-value and mitochondrial morphology analyzed by mitochondrial fragmentation count (MFC) respectively after (b, f) No treatment (c, g) E2-biotin (d, h) UVA and (e, i) UVA + E2-biotin treatments in *NQO1*$^{+/+}$ *and NQO1*$^{-/-}$ cells (n = 30 cells counted per condition, *p < 0.05). (j) Mitochondrial and (k) nuclear DNA damage quantified by LA-qPCR in *NQO1*$^{+/+}$ *and NQO1*$^{-/-}$ cells 24 h post-UVA (5 J/cm^2) (n = 3, *p < 0.05). (l) Western blot and quantification of CYP1B1 in the mitochondrial fractions of *NQO1*$^{+/+}$ *and NQO1*$^{-/-}$ cells at 24 h post-UVA (n = 3, *p < 0.05). (m) Representative Western blot image and quantification of cytochrome *c* release in the whole cell lysate at 24 h post E2-biotin (n = 3, *p < 0.05).

within mitochondria for *NQO1*$^{+/+}$ and *NQO1*$^{-/-}$ cell lines, suggesting the absence of mtDNA damage (Fig. 6b). However, *NQO1*$^{-/-}$ cells had a significantly higher colocalization of ARP with mitochondria after estrogen (R = 0.34, Fig. 6c), UVA (R = 0.64, Fig. 6d) and UVA with E2-biotin (E2-biotin + UVA) treatments (R = 0.68, Fig. 6e) compared to *NQO1*$^{+/+}$. This suggests that the absence of NQO1 enhanced the formation of estrogen-mediated apurinic sites, contributing to mitochondrial genotoxicity post UVA.

Next, we assessed the mitochondrial fragmentation and found that at baseline or with E2-biotin alone, there were no differences in the mitochondrial fragmentation count (MFC) of *NQO1*$^{+/+}$ and *NQO1*$^{-/-}$ cells (Fig. 6f and g); however, after UVA alone or E2-biotin + UVA treatments, the MFC was significantly greater in *NQO1*$^{-/-}$ compared to *NQO1*$^{+/+}$ cells (Fig. 6h and i). We also analyzed the mitochondrial morphology of the cell lines individually after each treatment (Supplementary Fig. 8c) and determined that UVA alone or E2-biotin + UVA, but not E2-biotin alone, caused a significant increase in the MFC of both *NQO1*$^{+/+}$ and *NQO1*$^{-/-}$ cells compared to no treatment (Supplementary Figs. 8d and e). To further investigate mtDNA damage, we quantified lesions/damage using LA-qPCR and found that after exposure to 5 J/cm^2 UVA, *NQO1*$^{-/-}$ had 1.34-fold decreased mtDNA amplification (Fig. 6j) and 2-fold decreased nDNA amplification (Fig. 6k) compared to *NQO1*$^{+/+}$ cells. Similarly, higher UVA dose of 10 J/cm^2 in *NQO1*$^{-/-}$ cells had 2.38-fold and 2.69-fold decreased mtDNA and nDNA amplification

respectively, compared to *NQO1*$^{+/+}$ cells (Supplementary Figs. 8f and g), indicating greater levels of both mtDNA and nDNA in the absence of NQO1.

Our previous publication reported that CYP1B1 translocates to mitochondria at 24 h post-UVA *in vitro*, potentially leading to estrogen-DNA adduct formation [7]. Herein, we detected a significant increase (2.5-fold) in CYP1B1 mitochondrial translocation for the *NQO1*$^{-/-}$ cell line post-UVA (5 J/cm^2) compared to that seen in *NQO1*$^{+/+}$ (Fig. 6l). Various other studies have implicated the role of CYP1B1 in mitochondria-mediated apoptosis using a cyto c release assay [51–53]. There was no significant difference in cytochrome *c* release after E2-Biotin in *NQO1*$^{+/+}$ cells (Fig. 6m); however, there was a significant increase (1.8-fold) in cytochrome *c* release after E2-Biotin in *NQO1*$^{-/-}$ cells (Fig. 6m) 24 h post treatment. This suggests that estrogen colocalization into mitochondria likely produces a substrate for mitochondrial CYP1B1 and leads to mtDNA damage and mitochondrial apoptosis, providing a mechanism for endo-degeneration in *Nqo1*-nulls. Studies on measuring actual estrogen-DNA adducts in mitochondrial fractions in response to UVA are needed in the future.

4. Discussion

The contribution of sex in the pathogenesis of many degenerative diseases, including FECD [9–11], has been an understudied area that is now gaining momentum in explaining the sex differences in prevalence and outcomes of many age-related disorders. Recently, female predominance was reported in age-related macular degeneration (AMD) [54] and linked to the levels of complement factors that vary by sex, shedding light on sex as a risk factor for the development of AMD. Specifically, complement factor B and I were significantly higher in females than males for the intermediate phenotype of AMD. Similarly, neurological diseases are also associated with sex differences in prevalence and disease manifestation [55–57], in which, females have a two-fold increased risk for developing dementia in Alzheimer's [58] and a 2.3-fold increase in multiple sclerosis prevalence [59]. Studies also show that the female sex is the most significant risk factor for Alzheimer's disease, independent of survival rates and age-adjusted risk. Specifically, female-specific reproductive history factors such as estrogen metabolism in the pre- or post-menopause significantly contribute to Alzheimer's disease risk [60]. In general, endogenous estrogen has been shown to have an effect on sex-specific processes, such as the development of the female phenotype during germ cell maturation, pregnancy, and other physiological processes in the cardiovascular and nervous systems [61]. However, augmented estrogen exposure through hormonal replacement therapy increases the risk of dementia in postmenopausal women [62]. In other diseases such as breast cancer, selective estrogen receptor modulators are clinically prescribed to suppress toxic endogenous estrogen production [63]. In contrast to the detrimental effects of estrogen, many studies have suggested neuroprotective functions of estrogen in diseases like stroke [64,65] and Alzheimer's disease [66]. The search for biological variables has identified a complex interplay between the neuroprotective effects of estrogen and the detrimental effects of a self-perpetuating toxic cascade of estradiol metabolism; both processes are involved in the degenerative process of neurological conditions. In the ongoing 'tug of war', excessive reactive estrogen quinones often offset the antioxidant and anti-apoptotic effects generated by estrogen and further aggravate the pathological conditions [67].

Building upon previous studies on the causative effects of UVA on FECD development, we demonstrate heightened susceptibility of *Nqo1*-null mice, and, particularly, *Nqo1*-null female mice to UVA-induced CEnC loss. Although previous studies have shown greater susceptibility of *Nqo1*-null mice to oxidative stress [68], and menadione-induced toxicity [68], the female sex has not been specifically investigated in these studies. The compounding effects of increased ROS production to the lack estrogen quinone neutralization (in the absence of NQO1) is evident in the formation of a more 'extreme' FECD phenotype in *Nqo1*-null female compared to *Nqo1*-null male mice. Since both *Nqo1*--null females and males have lost their ROS neutralizing activity, we show that the differentiating factors between the phenotypic differences of sexes stem from upstream factors of reactive estrogen quinone production and are driven by the CYP family of enzymes. Indeed, there are sex differences in CYP isoform expression levels [33], and since CYP1B1 is ubiquitously and robustly expressed in ocular tissues [69], it has a more pronounced activity in female corneas leading to the formation of estrogen metabolism byproducts causing a more pronounced damage in females. Interestingly, we also show that estrogen accumulates in the aqueous fluid of the eye and becomes metabolized by ocular CYP1B1 into reactive metabolites causing CEnC loss. Analysis of human specimens corroborated the *in vitro* data by showing upregulation of CYP1B1-related toxic metabolites and DNA-adducts ($4OHE_{1/2}$) and downregulation of non-toxic CYP1B1-related catechol conjugates ($4\text{-}OCH_3E_{1/2}$) in human FECD aqueous humor and tissues.

We further mimicked the female phenotype of endo-degeneration by exogenous estrogen injection of male mice and showed that estrogen-induced CEnC loss in males was mitigated by deletion of CYP1B1 in male mice, pointing to the metabolite-dependent effect. Although *Cyp1b1*-null mice did not show a difference in susceptibility to UVA compared to wild type mice, the 'stress' of estrogen injection clearly differentiated the ability to metabolize estrogen between *Cyp1b1*-wild-type and *Cyp1b1*-null males, pointing directly to the cytotoxic effects of estrogen on endo-degeneration in the cornea. Alternatively, ovariectomized mice could be used to provide future proof-of-concept studies on estrogen toxicity in both wild-type and *Nqo1*-null mice [70].

The detrimental effects of estrogen metabolites have been established in breast cancer, where CYP1B1-mediated DNA adducts resulted in the formation of harmful estrogen-adducts; thus, initiating carcinogenesis [71]. Specifically, serum estrogen DNA adducts such as $4OHE_{1/2}$ DNA adducts produced in large quantities can be used as potential biomarkers for breast [72] and ovarian [73] cancers. Similarly, a correlation of CYP1B1-mediated DNA adducts with carcinogenesis was shown that correlated with a significant reduction in lymphomas in *Cyp1b1*$^{-/-}$ compared to wild-type mice [47]. Others showed significantly higher amounts of estrogen metabolites and adducts in the urine samples of Parkinson's patients compared to controls, suggesting that the imbalance in estrogen metabolism could initiate neurodegeneration [74]. Furthermore, a CYP1B1 polymorphism [71] has been shown to contribute to the development of breast [75], lung [76], head and neck [77] cancers.

To ameliorate the deleterious effects of ROS and estrogen quinones, we utilized a targeted CYP1B1 inhibitor, TMS, and a broader acting NRF2 agonist and CYP1B1 inhibitor, berberine, and showed cytoprotective effects of both compounds in rescuing the FECD phenotype. By utilizing female mice, which harbor the most severe phenotype, we showed that TMS rescued cell loss not only in *Nqo1*$^{+/+}$ but also in *Nqo1*$^{-/-}$ mice, indicating that targeting estrogen metabolite formation is consistent with the underlying mechanism of cell loss. This data is supported by other studies, where CYP1B1 inhibition ameliorates diabetes [78], hypertension [79], decreases tumorigenesis [69] improves renal and cardiovascular functions [80] and prevents development of pulmonary hypertension [81]. We found no significant differences in corneal thickness across different genotypes of *Nqo1*$^{+/+}$and *Nqo1*$^{-/-}$ males and females after UVA because we utilized a lower dose of UVA that does not cause sufficient CEnC damage to trigger corneal edema. This is supported by earlier studies where no corneal edema was detected with significant loss of CEnC in lower grade Fuchs patients [82].

Nuclear erythroid 2-related factor 2 (NRF2) is a transcription factor that binds to the antioxidant response element (ARE) and induces transcription of many antioxidants and cytoprotective enzymes, including NQO1, and has the effect of preventing cancer initiation by detoxifying toxic estrogen quinones [83]. Berberine being a NRF2/ARE

pathway activator demonstrates therapeutic effects against many chronic diseases, such as obesity, diabetes, inflammatory bowel disease, atherosclerosis, and cardiovascular diseases, due to its multiple-target effects [84]. Specifically, berberine has been shown to activate NRF2/ARE signaling and exert cytoprotection in non-alcoholic fatty liver disease [85], and many neurological and metabolic diseases [86–88]. In healthy male humans, repeated administration of berberine decreased CYP2D6, CYP2C9, and CYP3A4 [89] compared to placebo. Berberine had the most potent and selective inhibitory effect on CYP1B1 with the lowest dissociation constant (Ki) value of 44 nM compared to other CYP isoforms. Moreover, berberine inhibits polymorphic variants of CYP1B1 (CYP1B11.1) by forming hydrogen-bonding interaction of Asp 228 on CYP1B1.1 with the methoxy moiety of berberine [49]. The quite dramatic rescue of cell phenotype with berberine in the FECD model indicates that mitigating ongoing oxidative stress along with the harmful effects of quinone metabolism is a promising rescue strategy for FECD.

Mitochondrial DNA (mtDNA) damage and altered mitochondrial function play a key role in CEnC dysfunction in FECD [90]. The main differentiating factor in greater female susceptibility to UVA-induced cells loss, has been the persistence of mtDNA damage in female but not male mice [7]. In this study, we show that UVA induces estrogen metabolism that is responsible for greater mtDNA damage seen in females. Moreover, CYP1B1 activation had a differentiating effect in inducing a more severe mtDNA damage, as CYP1B1 deletion led to the reduction in estrogen metabolite production and in mtDNA, not nDNA, damage compared to estrogen-treated wild-type male mice. *In vitro* studies showed that estrogen translocates to mitochondria and causes apurinic sites, consistent with UVA-induced mtDNA damage and cytochrome C release. Interestingly, loss of NQO1 upon UVA irradiation augments DNA mutagenesis while increasing CYP1B1 translocation to the mitochondria. Studies have shown that CYP1B1 has an N-terminal mitochondrial targeting sequence (residues 41–48) enabling CYP1B1 mitochondrial translocation and causing mitochondrial dysfunction due to carcinogen and cigarette exposure [53,91]. Specifically, polycyclic aromatic hydrocarbon (PAH)-inducible CYP1B1 generates mitochondrial ROS, decreases total mtDNA content, and inhibits complex I activity in the lungs of wild-type mice but not in *Cyp1b1*-null mice [53]. Systemic exposure to PAH led to the mitochondrial translocation of CYP1B1 and increased the aryl hydrocarbon hydroxylation activity in the mitochondria of pulmonary tissues that was rescued by TMS [51]. Smoking exposure being one of the risk factors of FECD, renders pollutants like benzo(a)pyrene (BaP), very relevant in activation of CYPs in response to environmental exposures that are likely the epigenetic modifiers of FECD development [11,14].

Studies have shown that CYP1B1 either resides in the endoplasmic reticulum or the inner mitochondrial membrane where metabolism of different substrates leads to the modulation of cell function and apoptosis [92,93]. Similar to the notion that estrogen metabolism, albeit leading to harmful metabolites, is inducible in mitochondria, studies have shown that mitochondrial CYP1B1 is highly involved in neurosteroid pregnenolone production in the brain [94]. One of the pitfalls of our study is that we could not show the formation of estrogen metabolites in mitochondrial fractions due to the fast turnover of estrogen-DNA adducts causing loss during the mitochondrial preparation steps. However, the fact that apurinic sites colocalized to mitochondria were augmented in the estrogen-treated cells indicates indirectly the causal relationship between estrogen and DNA mutagenesis, elucidating the cause of greater mtDNA damage seen in females after UVA.

This is the first study that provides mechanistic insight into the crosstalk of an estrogen metabolizing enzyme, CYP1B1, and an antioxidant and estrogen quinone detoxifying enzyme, NQO1, in response to UV light-induced endo-degeneration in FECD pathogenesis. The presence of ongoing oxidative stress, as seen with the loss of NQO1, potentiates the harmful effects of estradiol and leads to chronic estrogen cytotoxicity, leading to exacerbation of FECD in females. Moreover, mitochondrial DNA damage likely provides the link between the harmful effects of estrogen metabolism and oxidative stress in females developing FECD. Our study opens the therapeutic option for pharmacological agents that can simultaneously upregulate NQO1, downregulate CYP1B1 and ameliorate CEnC degeneration in FECD.

Author contributions

VK, ND and UVJ designed, performed the study, and wrote the manuscript. MP, RW, SA, MZ, HH, AM, SK collected and analyzed the data. UVJ, ER, FJG, MOP, and FWP reviewed and approved the final version. MOP and FWP provided the human FECD tissues. The authors would like to thank Mrs. Jaini Parekh (https://jainiparekh.com/) for figure illustrations.

Significance

Fuchs endothelial corneal dystrophy (FECD) is a female-predominant oxidative stress disorder that is the leading cause of corneal transplantation worldwide with no available pharmacological treatments. Thus, there is an unmet need to understand the disease pathogenesis with respect to female prevalence and oxidative stress in order to develop pharmacological interventions. Herein, we demonstrate that the absence of antioxidant enzyme NQO1 exacerbated the production of estrogen-metabolizing enzyme CYP1B1 and its related estrogen metabolites, as well as mitochondrial DNA damage in females, thereby explaining how crosstalk of CYP1B1 and NQO1 drives sex-dependent differences in corneal endothelial (CE) susceptibility to ultraviolet A (UVA)-induced FECD. This study underscores the importance of impaired estrogen metabolism and oxidant-antioxidant imbalance in CEnC degeneration for FECD development.

Declaration of competing interest

None.

Data availability

Data will be made available on request.

Acknowledgments

We acknowledge Prof. Irene Kochevar and Bill A. Farinelli (Wellman Center for Photomedicine, Massachusetts General Hospital, Harvard Medical School, Boston) for their expertise in UVA lamp assembly and *in vivo* irradiation. The work was supported by NIH/NEI R01EY020581 (to U.V.J.) and K99EY031339 (to V.K.) and in part by the National Cancer Institute (NCI) Intramural Research Program (to F.J.G.).

Appendix A. Supplementary data

Supplementary data to this article can be found online at https://doi.org/10.1016/j.redox.2023.102986.

References

[1] N.C. Joyce, Proliferative capacity of the corneal endothelium, Prog. Retin. Eye Res. 22 (2003) 359–389.
[2] T. Schmedt, M.M. Silva, A. Ziaei, U. Jurkunas, Molecular bases of corneal endothelial dystrophies, Exp. Eye Res. 95 (2012) 24–34.
[3] U.V. Jurkunas, Fuchs endothelial corneal dystrophy through the prism of oxidative stress, Cornea 37 (Suppl 1) (2018) S50–S54.
[4] U.V. Jurkunas, M.S. Bitar, T. Funaki, B. Azizi, Evidence of oxidative stress in the pathogenesis of fuchs endothelial corneal dystrophy, Am. J. Pathol. 177 (2010) 2278–2289.
[5] V.M. Borderie, M. Baudrimont, A. Vallee, T.L. Ereau, F. Gray, L. Laroche, Corneal endothelial cell apoptosis in patients with Fuchs' dystrophy, Invest. Ophthalmol. Vis. Sci. 41 (2000) 2501–2505.

[6] Q.J. Li, et al., The role of apoptosis in the pathogenesis of Fuchs endothelial dystrophy of the cornea, Arch. Ophthalmol. 119 (2001) 1597–1604.
[7] C. Liu, et al., Ultraviolet A light induces DNA damage and estrogen-DNA adducts in Fuchs endothelial corneal dystrophy causing females to be more affected, Proc. Natl. Acad. Sci. U.S.A. 117 (2020) 573–583.
[8] H.S. Son, G. Villarreal Jr., H. Meng, C.G. Eberhart, A.S. Jun, On the origin of 'guttae', Br. J. Ophthalmol. 98 (2014) 1308–1310.
[9] P. Yeh, K. Colby, Corneal endothelial dystrophies, in: 4th. ed., in: C. Foster, T. Dimitri (Eds.), The Cornea: Scientific Foundations and Clinical Practice, vol. 47, Lippincott William and Wilkins, Philadelphia, 2005, p. 849.
[10] S.E. Wilson, W.M. Bourne, Fuchs' dystrophy, Cornea 7 (1988) 2–18.
[11] G.M. Zoega, et al., Prevalence and risk factors for cornea guttata in the Reykjavik Eye Study, Ophthalmology 113 (2006) 565–569.
[12] E.D. Wieben, et al., A common trinucleotide repeat expansion within the transcription factor 4 (TCF4, E2-2) gene predicts Fuchs corneal dystrophy, PLoS One 7 (2012), e49083.
[13] P. Gain, et al., Global survey of corneal transplantation and eye banking, JAMA Ophthalmol. 134 (2016) 167–173.
[14] X. Zhang, et al., Association of smoking and other risk factors with Fuchs' endothelial corneal dystrophy severity and corneal thickness, Invest. Ophthalmol. Vis. Sci. 54 (2013) 5829–5835.
[15] K. Kitagawa, et al., Prevalence of primary cornea guttata and morphology of corneal endothelium in aging Japanese and Singaporean subjects, Ophthalmic Res. 34 (2002) 135–138.
[16] N.A. Afshari, A.B. Pittard, A. Siddiqui, G.K. Klintworth, Clinical study of Fuchs corneal endothelial dystrophy leading to penetrating keratoplasty: a 30-year experience, Arch. Ophthalmol. 124 (2006) 777–780.
[17] S.W.S. Chan, Y. Yucel, N. Gupta, New trends in corneal transplants at the University of Toronto, Can. J. Ophthalmol. 53 (2018) 580–587.
[18] C. Liu, Y. Chen, I.E. Kochevar, U.V. Jurkunas, Decreased DJ-1 leads to impaired Nrf2-regulated antioxidant defense and increased UV-A-induced apoptosis in corneal endothelial cells, Invest. Ophthalmol. Vis. Sci. 55 (2014) 5551–5560.
[19] C. Liu, D. Vojnovic, I.E. Kochevar, U.V. Jurkunas, UV-A irradiation activates Nrf2-regulated antioxidant defense and induces p53/caspase3-dependent apoptosis in corneal endothelial cells, Invest. Ophthalmol. Vis. Sci. 57 (2016) 2319–2327.
[20] M.S. Bitar, C. Liu, A. Ziaei, Y. Chen, T. Schmedt, U.V. Jurkunas, Decline in DJ-1 and decreased nuclear translocation of Nrf2 in Fuchs endothelial corneal dystrophy, Invest. Ophthalmol. Vis. Sci. 53 (2012) 5806–5813.
[21] U.V. Jurkunas, et al., Decreased expression of peroxiredoxins in Fuchs' endothelial dystrophy, Invest. Ophthalmol. Vis. Sci. 49 (2008) 2956–2963.
[22] A. Halilovic, et al., Menadione-induced DNA damage leads to mitochondrial dysfunction and fragmentation during rosette formation in fuchs endothelial corneal dystrophy, Antioxidants Redox Signal. 24 (2016) 1072–1083.
[23] P. Czarny, et al., DNA damage and repair in Fuchs endothelial corneal dystrophy, Mol. Biol. Rep. 40 (2013) 2977–2983.
[24] P. Czarny, et al., Mutagenesis of mitochondrial DNA in Fuchs endothelial corneal dystrophy, Mutat. Res. 760 (2014) 42–47.
[25] L.V. Favreau, C.B. Pickett, The rat quinone reductase antioxidant response element. Identification of the nucleotide sequence required for basal and inducible activity and detection of antioxidant response element-binding proteins in hepatoma and non-hepatoma cell lines, J. Biol. Chem. 270 (1995) 24468–24474.
[26] P. Nioi, M. McMahon, K. Itoh, M. Yamamoto, J.D. Hayes, Identification of a novel Nrf2-regulated antioxidant response element (ARE) in the mouse NAD(P)H: quinone oxidoreductase 1 gene: reassessment of the ARE consensus sequence, Biochem. J. 374 (2003) 337–348.
[27] A.T. Dinkova-Kostova, P. Talalay, NAD(P)H:quinone acceptor oxidoreductase 1 (NQO1), a multifunctional antioxidant enzyme and exceptionally versatile cytoprotector, Arch. Biochem. Biophys. 501 (2010) 116–123.
[28] N.W. Gaikwad, E.G. Rogan, E.L. Cavalieri, Evidence from ESI-MS for NQO1-catalyzed reduction of estrogen ortho-quinones, Free Radic. Biol. Med. 43 (2007) 1289–1298.
[29] X. He, M.G. Chen, G.X. Lin, Q. Ma, Arsenic induces NAD(P)H-quinone oxidoreductase I by disrupting the Nrf2 x Keap1 x Cul3 complex and recruiting Nrf2 x Maf to the antioxidant response element enhancer, J. Biol. Chem. 281 (2006) 23620–23631.
[30] T. Miyajima, et al., Loss of NQO1 generates genotoxic estrogen-DNA adducts in fuchs endothelial corneal dystrophy, Free Radic. Biol. Med. 147 (2020) 69–79.
[31] E.L. Cavalieri, E.G. Rogan, Unbalanced metabolism of endogenous estrogens in the etiology and prevention of human cancer, J. Steroid Biochem. Mol. Biol. 125 (2011) 169–180.
[32] E. Cavalieri, et al., Catechol estrogen quinones as initiators of breast and other human cancers: implications for biomarkers of susceptibility and cancer prevention, Biochim. Biophys. Acta 1766 (2006) 63–78.
[33] J. Hakkola, et al., Expression of CYP1B1 in human adult and fetal tissues and differential inducibility of CYP1B1 and CYP1A1 by Ah receptor ligands in human placenta and cultured cells, Carcinogenesis 18 (1997) 391–397.
[34] P. Pelkonen, M. Lang, M. Pasanen, Tissue and sex-dependent differences in CYP2A activities in hamsters, Arch. Toxicol. 68 (1994) 416–422.
[35] T. Miyai, et al., Activation of PINK1-parkin-mediated mitophagy degrades mitochondrial quality control proteins in fuchs endothelial corneal dystrophy, Am. J. Pathol. 189 (2019) 2061–2076.
[36] S.L. Byers, M.V. Wiles, S.L. Dunn, R.A. Taft, Mouse estrous cycle identification tool and images, PLoS One 7 (2012), e35538.
[37] A.K. Johansen, et al., The serotonin transporter promotes a pathological estrogen metabolic pathway in pulmonary hypertension via cytochrome P450 1B1, Pulm. Circ. 6 (2016) 82–92.
[38] S. Thirunavukkarasu, et al., Cytochrome P450 1B1 contributes to the development of angiotensin II-induced aortic aneurysm in male apoe(-/-) mice, Am. J. Pathol. 186 (2016) 2204–2219.
[39] N. Ziegler, et al., Beta-catenin is required for endothelial Cyp1b1 regulation influencing metabolic barrier function, J. Neurosci. 36 (2016) 8921–8935.
[40] N.I. El-Desouki, G.A. Tabl, Y.A. Elkhodary, Biological studies on the effect of estrogen on experimentally induced asthma in mice, Toxicol. Ind. Health 32 (2016) 30–38.
[41] G.E. Saraceno, M.J. Bellini, L.M. Garcia-Segura, F. Capani, Estradiol activates PI3K/Akt/GSK3 pathway under chronic neurodegenerative conditions triggered by perinatal asphyxia, Front. Pharmacol. 9 (2018) 335.
[42] K. Tripathi, et al., Detection and evaluation of estrogen DNA-adducts and their carcinogenic effects in cultured human cells using biotinylated estradiol, Mol. Carcinog. 56 (2017) 1010–1020.
[43] J.H. Santos, B.S. Mandavilli, B. Van Houten, Measuring oxidative mtDNA damage and repair using quantitative PCR, Methods Mol. Biol. 197 (2002) 159–176.
[44] B. Mondal, H. Chen, W. Wen, E.L. Cavalieri, E.G. Rogan, M. Zahid, Modulation of cellular response to arsenic trioxide toxicity by resveratrol, ACS Omega 3 (2018) 5511–5515.
[45] V.O. Okoh, et al., Redox signalling to nuclear regulatory proteins by reactive oxygen species contributes to oestrogen-induced growth of breast cancer cells, Br. J. Cancer 112 (2015) 1687–1702.
[46] V.O. Okoh, Q. Felty, J. Parkash, R. Poppiti, D. Roy, Reactive oxygen species via redox signaling to PI3K/AKT pathway contribute to the malignant growth of 4-hydroxy estradiol-transformed mammary epithelial cells, PLoS One 8 (2013), e54206.
[47] J. Buters, et al., CYP1B1 determines susceptibility to low doses of 7,12-dimethyl-benz[a]anthracene-induced ovarian cancers in mice: correlation of CYP1B1-mediated DNA adducts with carcinogenicity, Carcinogenesis 24 (2003) 327–334.
[48] M. Zahid, N.W. Gaikwad, E.G. Rogan, E.L. Cavalieri, Inhibition of depurinating estrogen-DNA adduct formation by natural compounds, Chem. Res. Toxicol. 20 (2007) 1947–1953.
[49] S.N. Lo, Y.P. Chang, K.C. Tsai, C.Y. Chang, T.S. Wu, Y.F. Ueng, Inhibition of CYP1 by berberine, palmatine, and jatrorrhizine: selectivity, kinetic characterization, and molecular modeling, Toxicol. Appl. Pharmacol. 272 (2013) 671–680.
[50] Y. Deng, et al., Berberine attenuates hepatic oxidative stress in rats with non-alcoholic fatty liver disease via the Nrf2/ARE signalling pathway, Exp. Ther. Med. 17 (2019) 2091–2098.
[51] D.N. Das, et al., Elimination of dysfunctional mitochondria through mitophagy suppresses benzo[a]pyrene-induced apoptosis, Free Radic. Biol. Med. 112 (2017) 452–463.
[52] Z. Yu, et al., Mitochondrial cytochrome P450 (CYP) 1B1 is responsible for melatonin-induced apoptosis in neural cancer cells, J. Pineal Res. 65 (2018), e12478.
[53] S. Bansal, et al., Mitochondrial targeting of cytochrome P450 (CYP) 1B1 and its role in polycyclic aromatic hydrocarbon-induced mitochondrial dysfunction, J. Biol. Chem. 289 (2014) 9936–9951.
[54] A.I. Marin, et al., Sex and age-related differences in complement factors among patients with intermediate age-related macular degeneration, Transl. Vis. Sci. Technol. 11 (2022) 22.
[55] P. Honarpisheh, L.D. McCullough, Sex as a biological variable in the pathology and pharmacology of neurodegenerative and neurovascular diseases, Br. J. Pharmacol. 176 (2019) 4173–4192.
[56] J.L. Podcasy, C.N. Epperson, Considering sex and gender in Alzheimer disease and other dementias, Dialogues Clin. Neurosci. 18 (2016) 437–446.
[57] J.A. Clayton, Sex influences in neurological disorders: case studies and perspectives, Dialogues Clin. Neurosci. 18 (2016) 357–360.
[58] S. Seshadri, et al., Lifetime risk of dementia and Alzheimer's disease. The impact of mortality on risk estimates in the Framingham Study, Neurology 49 (1997) 1498–1504.
[59] C. Ahlgren, A. Oden, J. Lycke, High nationwide prevalence of multiple sclerosis in Sweden, Mult. Scler. 17 (2011) 901–908.
[60] S. Jett, et al., Endogenous and exogenous estrogen exposures: how women's reproductive health can drive brain aging and inform alzheimer's prevention, Front. Aging Neurosci. 14 (2022), 831807.
[61] J. Cui, Y. Shen, R. Li, Estrogen synthesis and signaling pathways during aging: from periphery to brain, Trends Mol. Med. 19 (2013) 197–209.
[62] S.A. Shumaker, et al., Estrogen plus progestin and the incidence of dementia and mild cognitive impairment in postmenopausal women: the Women's Health Initiative Memory Study: a randomized controlled trial, JAMA 289 (2003) 2651–2662.
[63] K.C. An, Selective estrogen receptor modulators, Asian Spine J 10 (2016) 787–791.
[64] D.W. Brann, K. Dhandapani, C. Wakade, V.B. Mahesh, M.M. Khan, Neurotrophic and neuroprotective actions of estrogen: basic mechanisms and clinical implications, Steroids 72 (2007) 381–405.
[65] P.D. Hurn, I.M. Macrae, Estrogen as a neuroprotectant in stroke, J. Cerebr. Blood Flow Metabol. 20 (2000) 631–652.
[66] J.W. Simpkins, E. Perez, X. Wang, S. Yang, Y. Wen, M. Singh, The potential for estrogens in preventing Alzheimer's disease and vascular dementia, Ther. Adv. Neurol. Disord. 2 (2009) 31–49.
[67] J. Nilsen, Estradiol and neurodegenerative oxidative stress, Front. Neuroendocrinol. 29 (2008) 463–475.
[68] V. Radjendirane, et al., Disruption of the DT diaphorase (NQO1) gene in mice leads to increased menadione toxicity, J. Biol. Chem. 273 (1998) 7382–7389.
[69] V. Vasiliou, F.J. Gonzalez, Role of CYP1B1 in glaucoma, Annu. Rev. Pharmacol. Toxicol. 48 (2008) 333–358.

[70] Y.H. Sniekers, H. Weinans, S.M. Bierma-Zeinstra, J.P. van Leeuwen, G.J. van Osch, Animal models for osteoarthritis: the effect of ovariectomy and estrogen treatment - a systematic approach, Osteoarthritis Cartilage 16 (2008) 533–541.
[71] A.R. Belous, D.L. Hachey, S. Dawling, N. Roodi, F.F. Parl, Cytochrome P450 1B1-mediated estrogen metabolism results in estrogen-deoxyribonucleoside adduct formation, Cancer Res. 67 (2007) 812–817.
[72] S. Pruthi, et al., Evaluation of serum estrogen-DNA adducts as potential biomarkers for breast cancer risk, J. Steroid Biochem. Mol. Biol. 132 (2012) 73–79.
[73] M. Zahid, C.L. Beseler, J.B. Hall, T. LeVan, E.L. Cavalieri, E.G. Rogan, Unbalanced estrogen metabolism in ovarian cancer, Int. J. Cancer 134 (2014) 2414–2423.
[74] N.W. Gaikwad, D. Murman, C.L. Beseler, M. Zahid, E.G. Rogan, E.L. Cavalieri, Imbalanced estrogen metabolism in the brain: possible relevance to the etiology of Parkinson's disease, Biomarkers 16 (2011) 434–444.
[75] M. Ociepa-Zawal, B. Rubis, V. Filas, J. Breborowicz, W.H. Trzeciak, Studies on CYP1A1, CYP1B1 and CYP3A4 gene polymorphisms in breast cancer patients, Ginekol. Pol. 80 (2009) 819–823.
[76] P.F. Chen, X.F. He, G.H. Huang, W. Wang, Z.H. Qiu, Association between the CYP1B1 polymorphisms and lung cancer risk: a meta-analysis, Technol. Cancer Res. Treat. 15 (2016) NP73–82.
[77] E.G. Shatalova, A.J. Klein-Szanto, K. Devarajan, E. Cukierman, M.L. Clapper, Estrogen and cytochrome P450 1B1 contribute to both early- and late-stage head and neck carcinogenesis, Cancer Prev. Res. 4 (2011) 107–115.
[78] X. Liu, et al., CYP1B1 deficiency ameliorates obesity and glucose intolerance induced by high fat diet in adult C57BL/6J mice, Am. J. Transl. Res. 7 (2015) 761–771.
[79] F.A. Yaghini, et al., Angiotensin II-induced vascular smooth muscle cell migration and growth are mediated by cytochrome P450 1B1-dependent superoxide generation, Hypertension 55 (2010) 1461–1467.
[80] B.L. Jennings, et al., Cytochrome P450 1B1 contributes to increased blood pressure and cardiovascular and renal dysfunction in spontaneously hypertensive rats, Cardiovasc. Drugs Ther. 28 (2014) 145–161.
[81] K. White, et al., Activity of the estrogen-metabolizing enzyme cytochrome P450 1B1 influences the development of pulmonary arterial hypertension, Circulation 126 (2012) 1087–1098.
[82] L.J. Kopplin, et al., Relationship of Fuchs endothelial corneal dystrophy severity to central corneal thickness, Arch. Ophthalmol. 130 (2012) 433–439.
[83] A. Giudice, et al., Dissecting the prevention of estrogen-dependent breast carcinogenesis through Nrf2-dependent and independent mechanisms, OncoTargets Ther. 12 (2019) 4937–4953.
[84] Y. Jin, D.B. Khadka, W.J. Cho, Pharmacological effects of berberine and its derivatives: a patent update, Expert Opin. Ther. Pat. 26 (2016) 229–243.
[85] P. Chen, Y. Li, L. Xiao, Berberine ameliorates nonalcoholic fatty liver disease by decreasing the liver lipid content via reversing the abnormal expression of MTTP and LDLR, Exp. Ther. Med. 22 (2021) 1109.
[86] J.W. Shou, P.C. Shaw, Therapeutic efficacies of berberine against neurological disorders: an update of pharmacological effects and mechanisms, Cells 11 (2022).
[87] J.W. Shou, C.K. Cheung, J. Gao, W.W. Shi, P.C. Shaw, Berberine protects C17.2 neural stem cells from oxidative damage followed by inducing neuronal differentiation, Front. Cell. Neurosci. 13 (2019) 395.
[88] Y. Dou, et al., Oxyberberine, an absorbed metabolite of berberine, possess superior hypoglycemic effect via regulating the PI3K/Akt and Nrf2 signaling pathways, Biomed. Pharmacother. 137 (2021), 111312.
[89] Y. Guo, Y. Chen, Z.R. Tan, C.D. Klaassen, H.H. Zhou, Repeated administration of berberine inhibits cytochromes P450 in humans, Eur. J. Clin. Pharmacol. 68 (2012) 213–217.
[90] V. Kumar, U.V. Jurkunas, Mitochondrial dysfunction and mitophagy in fuchs endothelial corneal dystrophy, Cells 10 (2021).
[91] H. Dong, et al., Mitochondrial targeting of mouse NQO1 and CYP1B1 proteins, Biochem. Biophys. Res. Commun. 435 (2013) 727–732.
[92] J. Yin, et al., Melatonin reprogramming of gut microbiota improves lipid dysmetabolism in high-fat diet-fed mice, J. Pineal Res. 65 (2018), e12524.
[93] H.K. Anandatheerthavarada, S. Addya, R.S. Dwivedi, G. Biswas, J. Mullick, N. G. Avadhani, Localization of multiple forms of inducible cytochromes P450 in rat liver mitochondria: immunological characteristics and patterns of xenobiotic substrate metabolism, Arch. Biochem. Biophys. 339 (1997) 136–150.
[94] Y.C. Lin, G. Cheung, Z. Zhang, V. Papadopoulos, Mitochondrial cytochrome P450 1B1 is involved in pregnenolone synthesis in human brain cells, J. Biol. Chem. 299 (2023), 105035.